INTEGRATION OF INERTIAL MEASUREMENT UNIT AND CAMERA FOR A VERTICAL LANDING AIRCRAFT ON A PATTERN

A THESIS SUBMITTED TO

THE SCHOOL OF GRADUATE STUDIES

OF

UNIVERSITY OF TURKISH AERONAUTICAL ASSOCIATION

BY

Andrew BUSINGYE

IN PARTIAL FULFILLMENT OF THE REQUIREMENTS
FOR THE DEGREE OF MASTER OF SCIENCE IN
MECHANICAL AND AERONAUTICAL ENGINEERING

AUGUST 2024

INTEGRATION OF INERTIAL MEASUREMENT UNIT AND CAMERA FOR A VERTICAL LANDING AIRCRAFT ON A PATTERN

A THESIS SUBMITTED TO
THE SCHOOL OF GRADUATE STUDIES
OF
UNIVERSITY OF TURKISH AERONAUTICAL ASSOCIATION

BY

Andrew BUSINGYE

IN PARTIAL FULFILLMENT OF THE REQUIREMENTS
FOR THE DEGREE OF MASTER OF SCIENCE IN
MECHANICAL AND AERONAUTICAL ENGINEERING

Supervisor: Assoc. Prof. Dr. Habib KANBEROĞLU

AUGUST 2024

Approval of the thesis:

INTEGRATION OF INERTIAL MEASUREMENT UNIT AND CAMERA FOR A VERTICAL LANDING AIRCRAFT ON A PATTERN

Submitted by **ANDREW BUSIINGYE** in partial fulfillment of the requirements for the degree of **Master of Science in Mechanical and Aeronautical Engineering**, University of Turkish Aeronautical Association by,

Assoc. Prof. Dr. Adnan GÜZEL
Dean, The School of Graduate Studies, UTAA _____________

Assoc. Prof. Dr. Hamit Tekin
Head of the Department,
Mechanical and Aeronautical Engineering _____________
A**ssoc. Prof. Dr. Habib KANBEROĞLU**
Supervisor, Computer Eng, UTAA _____________

Examining Committee Members:

Assoc. Prof. Dr. Habib KANBEROĞLU
Computer Eng, UTAA _____________

Assist. Prof. Dr. Aytun ONAY
Electrical and Computer Eng, UTAA _____________

Assoc. Prof. Dr. Orhan ERDEN
Industrial Design Eng, Gazi University _____________

Date: 01/08/2024

I hereby declare that all information in this document has been obtained and presented in accordance with academic rules and ethical conduct. I also declare that, as required by these rules and conduct, I have fully cited and referenced all material and results that are not original to this work.

Andrew BUSINGYE

ABSTRACT

INTEGRATION OF INERTIAL MEASUREMENT UNIT AND CAMERA FOR A VERTICAL LANDING AIRCRAFT ON A PATTERN

BUSINGYE, Andrew
Master of Science, Mechanical and Aeronautical Engineering
Supervisor: Assist. Prof. Dr. Habib Kanberoglu

[01/08/2024], 108 pages

This thesis presents an integrated system for achieving robust relative navigation of a flying vehicle mostly at low altitudes vertical landing approach. The integration combines stereo cameras, an Inertial Measurement Unit (IMU), and an extended Kalman filter (EKF) to estimate navigation parameters (attitude, velocity, and position).

The aim is to enhance the robustness and accuracy of the relative navigation system in an environment where inertial navigation system INS/GPS (Global Positioning System) integrations signals may not provide reliable navigation due to the external jamming signals. The integration of stereo cameras and IMU provides complementary strengthened information for relative navigation by estimating the velocity, position, and orientation of a flying vehicle relative to the known location of the pattern.

The simulated results show the errors of system is highly unstable when navigating with the pure INS and this makes it not reliable for the real navigating. Based on the instability of error propagations with pure INS and having no control from the external signal sources make INS/GPS expensive and difficult system calibrations.

Simulated results show that the integration of stereo cameras/INS using the extended Kalman filter provides real-time accurate estimates in the determination of flying vehicle orientation, velocity, and position for the relative navigation system since this integration causes stable error for relative navigation with respect to the pattern.

The stereo cameras provide visual information and direct measurements with respect to the target location which enhances collision avoidance and accurate position estimation. The IMU provides acceleration and angular velocity information of flying vehicles which are used for continuous position, velocity, and orientation vehicle estimation over time.

The employment of the extended Kalman filter is to fuse the information from IMU and cameras for continuous dynamic state estimation based on the sensor measurements and accountability for bias and noise from the sensor data.

Matlab simulated results show that the integration of stereo cameras and IMU using an extended Kalman filter provides a real and unbiased state estimation of a flying vehicle’s position, velocity, and orientation for it gives an inline output with nominal navigation for a relative navigation system. This makes an integration of a stereo camera and IMU for a vertical landing aircraft on a pattern reliable, accurate, and cheap calibration since it requires no external signal sources as GPS does.

ÖZ

ATALETSEL NAVİGASYON SİSTEMİ VE KAMERA VERİLERİNİN TÜMLEŞTİRİLMESİ BİR DESEN ÜSTÜNE DİKEY İNİŞ YAPAN UÇAK İÇİN

BUSINGYE, Andrew
Master of Science, Mechanical and Aeronautical Engineering

Tez Yöneticisi: Doç. Dr. Habib Kanberoglu
[01/08/2024], 108 sayf

Bu tez, çoğunlukla alçak irtifalarda dikey iniş yaklaşımında uçan bir aracın sağlam göreceli navigasyonunu sağlamak için entegre bir sistem sunmaktadır. Entegrasyon, navigasyon parametrelerini (tutum, hız ve konum) tahmin etmek için stereo kameraları, bir Atalet Ölçüm Birimi'ni (IMU) genişletilmiş bir Kalman filtresiyle (EKF) birleştirir.

Amaç, ataletsel navigasyon sistemi INS/GPS (Küresel Konumlandırma Sistemi entegrasyon sinyallerinin harici karıştırma sinyalleri nedeniyle güvenilir navigasyon sağlayamadığı bir ortamda ilgili navigasyon sisteminin sağlamlığını ve doğruluğunu arttırmaktır. Stereo kameralar ve IMU entegrasyonu sağlar) Uçan bir aracın bilinen konum konumuna göre konumunu ve yönelimini tahmin ederek göreceli navigasyon için tamamlayıcı, güçlendirilmiş bilgi.

Simüle edilen sonuçlar, saf INS ile navigasyon sırasında sistem hatalarının oldukça kararsız olduğunu ve bu durumun onu gerçek navigasyon için güvenilir kılmadığını göstermektedir. Saf INS ile hata yayılımının kararsızlığına bağlı olması ve harici sinyal kaynaklarından kontrolün olmaması INS/GPS'in sistem kalibrasyonlarını pahalı ve zor hale getirir.

Simüle edilmiş sonuçlar, stereo kameraların/INS'nin genişletilmiş Kalman filtresini kullanan entegrasyonunun, ilgili navigasyon sistemi için uçan araç yöneliminin, hızının ve konumunun belirlenmesinde gerçek zamanlı doğru tahminler sağladığını

göstermektedir; çünkü bu entegrasyon, göreceli navigasyon için sabit hataya neden olur. desene.

Stereo kameralar, çarpışmadan kaçınmayı ve doğru konum tahminini geliştiren, hedef konuma göre görsel bilgi ve doğrudan ölçümler sağlar. IMU, zaman içinde sürekli konum, hız ve araç yönelimi tahmini için kullanılan uçan araçların ivme ve açısal hız bilgilerini sağlar.

Genişletilmiş Kalman filtresinin kullanılması, sensör ölçümlerine ve sensör verilerinden gelen yanlılık ve gürültüye ilişkin hesap verebilirliğe dayalı olarak sürekli dinamik durum tahmini için IMU ve kameralardan gelen bilgilerin birleştirilmesidir.

Matlab benzetimli sonuçları, stereo kameraların ve IMU'nun genişletilmiş bir Kalman filtresi kullanılarak entegrasyonunun, uçan bir aracın konumu, hızı ve yönüne ilişkin gerçek ve tarafsız bir durum tahmini sağladığını ve ilgili bir navigasyon sistemi için INS/GPS navigasyonu ile hat içi çıktı verdiğini göstermektedir. . Bu, GPS'in yaptığı gibi herhangi bir harici sinyal kaynağı gerektirmediğinden, dikey iniş yapan bir uçak için stereo kamera ve IMU'nun güvenilir, doğru ve ucuz bir kalibrasyon modeli üzerinde entegrasyonunu sağlar.

ACKNOWLEDGMENTS

I would like to express my gratitude to my supervisor Doç.Dr. Habib KANBEROĞLU for his unlimited contribution, guidance, and insight from the start of this thesis till the end.

TABLE OF CONTENTS

LIST OF FIGURES

LIST OF TABLE

CHAPTER 1

INTRODUCTION

Integration of an inertial measurement unit (IMU) and stereo camera for a vertical landing of a flying vehicle on a pattern improves the accuracy and robustness of navigation systems. The fusion of these sensors integration using the inertial measurement unit (IMU) and filtering the undesired noise by using the Kalman filter enhances the position and obstacle identification and the overall navigation performance including vehicle attitude. Stereo cameras enable depth perception and provide visual information. The use of an inertial measurement unit (IMU), for this system assists in providing the angular velocities and acceleration data to estimate the flying vehicles' orientation. An IMU is composed of three-axis orthogonal gyroscopes and accelerometers. The inertial navigation system is said to be strap-down INS when the IMU is directly installed to the vehicle's body. INS is a real-time algorithm to estimate the position, orientation, and velocity of a flying vehicle by integrating the signal rates given by an IMU [1]. To determine the position and velocity double integration of nongravitational and gravitational acceleration from a three-axis accelerometer is performed. These sensors are all subjected to errors and noises which result in unstable results. To make smooth output in attitude, position, and velocity calculated by the stereo cameras and IMU, the deployment of Kalman filter to estimate the system process is an essential activity in minimization of sensor errors and noises hence optimizing the system output accuracy. Combining data from multiple self-signal-reliant sensors provide the system an increasted accuracy and robustness compared to individual sensor or multiple sensors that depends signals from external sources.

1.1 Navigation Systems Background

The navigation system is a method of determining and planning the movement from one place to another (Chiella, 2019). Navigation is categorized as either absolute or relative navigation systems. In this thesis, the relative navigation system is the main concern.

Navigation with relation to a local reference frame is referred to as relative navigation. We suggest that the local frame shift as the vehicle travels through its surroundings, creating a pose graph-based topological representation of the outside World [2], [3].

A relative navigation system that improves aircraft situational awareness during formation flying is detailed. A relative navigation system determines relative location and velocity by analyzing the disparity between signals from pairs of sensors installed on flying vehicles. The system is predicated on the global positioning system (GPS) and inertial navigation system (INS) navigation technologies that are widely used in aircraft. The method involves calibrating the relative INS position using relative GPS readings [3], [4].

In ancient times various methods of navigation were used. Among many, is to utilize dead reckoning to calculate the present position based on starting position, speed, and direction measurements. Dead reckoning involves taking the last known position and time, recording the average speed and heading since then, and calculating the present time. To calculate velocity components north and east, the speed must be resolved using the heading angle. The change in position is calculated by multiplying each position by the time of the previous one. Finally, the position changes are added to the initial position to determine the current position. An equivalent process can be undertaken using inertial sensors [1]. The inertial sensors are accelerometers and gyroscopes which can sense the translational and rotation movements relative to an inertial frame. Inertial navigation system has imapcted a lot as the main component for relative navigation system nevertheless the errors of the system has remarkebly identified over the time. As a solution to stablise those errors, the need of external systems come into existitance. The INS integration with global positioning system (GPS) acted as a very good choice in many cases. In flying vehicles, the inertial navigation system (INS) and its integrations provide the attitude, velocity, and position of the vehicle accurately however the system requires other sources of information and this information is likely to be affected by environmental factors. This shows that an inertial navigation system is not a stand-alone navigation component but involves other signal source systems or units. Global positioning system signals depend upon the signal strength from the inline satellite signals. It was studied that the signals for global positioning systems to be reliable at least four satellite signals are to be received by GPS and the inertial measurement unit information/readings to be reliable depends upon gyroscopes and accelerometer calibration and installation accuracy of the component. INS with its intagration sensors, provides absolute information that must be transformed to the relative coordinates using the appropriate transformation matrix. The relative information is often required for formation control applications and coordination [5], [6].

Though the integration of global positioning system signals with inertial measurement unit has become the standard approach for position and attitude information display identification, it was found that the inertial navigation multi-sensor fusion which involves global positioning system (GPS) and inertial measurement unit (IMU) is complex and expensive not suitable for some flying vehicles (Eric N. Johnson, 2007), [7], [8]. The [9], and [10] found that the implementation of a vision-based navigation system could be the way to enhance relative navigation system accuracy since the camera is a self-signal reliance. Vision-based navigation method is adopted for navigation relative to the known fixed reference. The target's horizontal and vertical positions in the image plane are measured noisily by the camera in each of these methods, and the position and velocity of the aircraft in relation to the target are then estimated using an Extended Kalman Filter (EKF). Changes in the range from the camera to the target seems to be harder to determine due to the difficulty of depth perception with monocular vision [11]. The difference between successive image frames is tiny when the air vehicle is flying straight and blurry at low altitudes towards a non-accelerating target, which leads to a poor estimate of the target's distance from the aircraft. Based on [12], [13] the mostly used navigation systems taking an example of inertial navigation systems (INS) with its integrations like global positioning(GPS), GLONASS a Russian global navigation system, and Galileo, which is all generalized as global navigation satellite systems (GNSS) are all external signal dependants, and these external signals are the environmental effects, the use of the signal self-reliant system could be the solution to this issues and hence the flying vehicle navigation safety achieved. The new algorithm of using a camera and inertial measurement unit (IMU),is expected enhencincing the orientation and attitude of a flying vehicle mainly at low altitudes. With the use of suitable signal filters like Kalman filters, will be helpful in state estimation of flying vehicles relative to the reference frame. Various state estimation methods are to be studied in order to choose the suitable method for air vehicles mostly at low altitudes. The integration of the inertial measurement unit and camera is expected to be the new reliable navigation system.

1.2 State Estimation Methods

In navigation systems mostly for flying vehicles, state estimate is a crucial aspect for providing accurate information about the aircraft's position, velocity, and attitude at a given time. This information is essential for safe and efficient flight, and also for various mission-critical tasks such as landing, and target tracking. There are several methods of state estimation.

Least square estimation method: it is a method used to estimate the state space by minimizing the sum of the squares of the differences between the predicted and

measured values. Least squares can be used in a wide variety of categorical applications, including curve fitting of data, parameter identification, and system model realization. Many examples from diverse fields fall under these categories, for instance determining the damping properties of a fluid-filled damper as a function of temperature identification of aircraft dynamic and static aerodynamic coefficients, orbit and attitude determination, position determination using triangulation, and modal identification of vibratory system [14], [15].

Kalman filter (KF): The Kalman filter is the most used state estimation method in navigation systems. This combines sensor noisy measurements with a dynamic model of aerial vehicles' motion to estimate the current dynamic state. Kalman filter is efficient for both linear and nonlinear time-varying systems using its variant classes like Extended Kalman filter (EKF), and Unscented Kalman filter(UKF). In navigation and positioning systems, filtering methods are derived from the measurement equation and the nonlinear equation of state. They work in distinct temporal intervals. With the help of measurements from the k-1th step, the Kalman filter can be used to estimate an object's error or status in the kth step. Utilizing data regarding the system's dynamics, Kalman filters [16], [17]. The extended Kalman filter (EKF) is used to linearize the object dynamics equations and observation equations in systems with nonlinear dynamics. Partial derivatives of nonlinear state functions or their Taylor series expansion are used to carry out linearization. Unscented Kalman Filter (UKF) is an alternative to the EKF. This filter is a recursive estimating filter, and it functions rather well on the statistical parameters of these models after they have undergone nonlinear transformations. Its properties satisfy the requirements of substantially nonlinear systems. The unscented transform (UT), on which UKF is based, transforms the state vector into a collection of weighted sigma points. The UKF algorithms then make use of these points. The UKF algorithm is a collection of formulas required for steps in prediction, invention, and correction. A different approach to the general filtering problem is based on the particle filter (PF), which draws sample particles and their weights from the probability density via sequential importance sampling [17].

1.3 Sensor Errors

It has been demonstrated that correlation-based stereo systems work well for tasks like creating elevation maps and robot navigation. The researcher offers a thorough examination of the main causes of mistake for stereo system in the context of vehicle's navigation. Found that there are three main categories of errors that are identified which are systematic error, misalignment error, and foreshortening error. Significant range errors result when the total disparity errors are greater than three-tenths of a pixel. After gaining an understanding of these causes of errors (Yalin Xiong). The demonstration of the stereo algorithm inaccuracy has to be eradicated. Stereo cameras can be combined with additional sensors, like Inertial Navigation Systems (INS), to provide a complete and accurate navigation system. Sensor fusion approaches can improve a system's overall resilience by mitigating individual sensors' limits. Using an inertial measurement unit (IMU) which is an INS component that uses accelerometers, and gyroscopes to estimate an vehicles' orientation in space. IMU outputs include measurements of acceleration, angular rate, and attitude. IMU like many other sensors expericence some of the errors due to the accelerarion rate and angular velocities of IMU accererometer and gyroscope sensitivity. The most common IMU errors are misalignments, scale factor, accelerometer, and gyroscope bias [4], [12].

An integration of INS/GPS impacted a lot in the navigation system for flying vehicles however there are some errors encountered in GPS-based relative navigation systems that can significantly impact the accuracy and reliability of navigation data. These errors can be Satellite Clock Errors caused by imperfections in the satellite's onboard clock and could cause discrepancies in the timing of the GPS signals, leading to position errors, Orbital Errors could cause inaccuracies in the reported position of the GPS satellites that can result into misleading information about the satellite's location, causing errors in the calculated position of the receiver. Ionospheric Delays cause variations in the ionosphere's density can delay GPS signals and is likely to result in errors in the calculated distance between the satellite and the receiver, leading to position inaccuracies and changes in the troposphere's temperature, pressure, and humidity these can cause errors in the signal travel time, affecting position accuracy [12], [18].

1.4 Calibraration Methods

In navigation it is crusial for the sensors to be calibarated for the accurate and reliable readings. The calibration of sensor can be categorized into intrinsic or exntrisic parameter calibrations. In computer vision and photogrammetry, camera calibration is an essential procedure that entails determining the intrinsic and extrinsic properties of a camera. Extrinsic characteristics specify the location and orientation of the camera in the world coordinate system, whereas intrinsic parameters include focal length, optical center, and lens distortion. The camera calibration tackles on calibration of both intrinsic and extrinsic parameters [19], [20]. Chassebord camera calibration is the most common calibration method used for camera calibration because of its effectiveness and simplicity. This method is done following some procedures like a checkerboard pattern is printed and placed in different orientations in front of the camera, the camera captures multiple images of the checkerboard from different angles, corner detection algorithms identify the corners of the squares in each image, these detected corners are then used to solve for the camera’s intrinsic and extrinsic parameters and when distance sensor is fused with the camera, the distance sensor calibration depends on the camera calibrated data. They provide in real-time accurate range measurements in large angular fields at height above the ground and enable vehicles to perform a wide range of tasks by fusing image data from the camera mounted on vehicles. Calibration of a single image using known geometry, it is useful when a single image is available and the geometry of the scene is known. Self-calibration methods use multiple images of a scene without any special calibration object [10], [20], [21]. In order to effectively use the data from the camera and laser range sensor, it is important to know their relative position and orientation from each other, which affects the geometric interpretation of its measurements [19]. The sensors are always prone to the envirnomental factors which includes pressure and temperature for revolving sensor components.

1.5 Methodology

Based on the performance and barriers that encounter the current INS navigation algorithms for relative navigation systems and their integrations, the integration of inertial measurement unit (IMU) and camera data fused by extended Kalman filter as a new navigation system for a vertical landing aircraft is expected to measure the attitude and altitude of the flying system with respect to the known pattern.

By the use of MATLAB environment, algorithm programming and simulation test of this new system is used to identify the flying vehicle velocity, position, and orientation behaviors and accuracy in comparison to the nominal navigation parameters and currently in use real INS/GPS navigation based hence aiming to enhance navigation accuracy of the flying vehicle that is not depending on the external signal sources.

CHAPTER 2

INERTIAL NAVIGATION SYSTEM

The inertial navigation system (INS) is a system cable for locating and orienting the vehicles. INS is composed of three-axis accelerometers and gyroscopes enabling the system to calculate the position and attitude of a flying vehicles. INS could be a solution for relative navigation or absolute navigation systems. For this case, INS for the relative navigation system is the basis of the study. INS for relative navigation systems, is an algorithm that continuously computes the flying vehicles' orientation, position, and velocity relative to the reference platform without external signal sources [4], [22], [2].

2.1 Inertial Navigation Systems Modeling

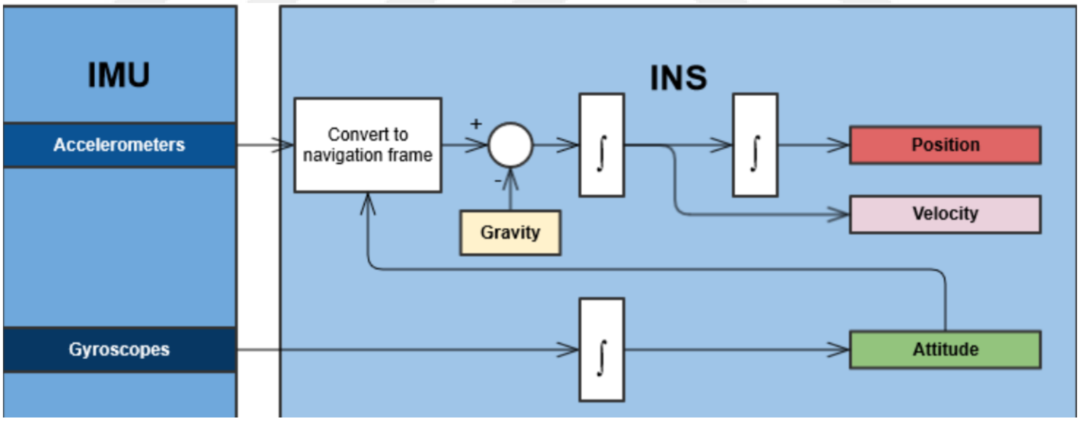

Figure 2 1**.** INS Model Diagram (Joong-hee Han 6 July 2020)

The figure 2.1 shows the pure INS performance in deteeermination of vehicles' orientation, position, and velocity by the use of system integrators that integrates inertial measurement unit (IMU) data.

Relative navigation systems for flying vehicles is important for mission accomplishment. The common flying vehicle navigation algorithms for relative navigation involves an inertial navigation system ((INS) and its integrations as the modern navigation system currently used. A pure INS works by integrating accelerometer data to calculate velocity and double integration accelerometer data to position a flying vehicle. Integrating the gyroscope data by INS the vehicle's attitude is determined based on the initial orientation, position, and velocity. The algorithm update over time is prone to sensor biases and imperfect sensor output scaling all lead to inaccurate readings. Since the output of the system is a result of integrating accelerometer and gyroscope data, this small integration repetitive error leads to drift error [1]. The integrations of INS were introduced due to the increased errors of the system with respect to time. To smoothen the system errors the system was integrated with other sensors/systems such as the global positioning system (GPS) [23], [24]. INS/GPS integration has played an essential role in the navigation of flying vehicles and in various robot control systems. Even though the use of the INS/GPS became a reasonable idea, there are some environments where GPS cannot operate positively since it is an external signal dependent. The way to reduce errors resulted in poor satellite signals to the GPS receiver, and the IMU bias the deployment of the Kalman filter to linearize the nonlinearized data [6], [25] the Kalman filter is updated with the GPS. In the circumstances where GPS reception is spotty, this arrangement has an edge. When the observed number of satellite signals does not reach four, loosely coupled filters are unable to provide filters with accurate data. Enhancing navigation accuracy by limiting drift during the INS cycle and under poor GPS signal reception, is possible through the vehicle state extension to incorporate IMU biases [6].

Inertial navigation system plays a big role in aerospace navigation systems using inertial sensor measurements for continuous vehicle navigation applications. Acellerommeter for identification of vehicle acceleration and velocities, gyroscope for the angular velocity measurements. Although the errors of the INS have remarkeble identified with time. The INS intergtartion algorithm for linearisation and fuse data from the fore mentioned sensors have stabolised the errors and makes it happen to identify the attitude and altitude of flying vehicle. The inertial navigation system modeling approches require the kinematic modeling since it involves the motion system. The involvement of intagration measured accelaration to estimate position and accelaration and the involvement of measured angular velocities in estimation of vehicle orientation. The system modeling considers also inertial navigation error modeling approach [13], [26]. Regardless of the current accuracy, the system encounters several errors like drift, bias, noises, and environmental factors, the approach to realizing error is aiming for accuracy enhancement for the more improved navigation system. Since the inertial navigation system is a not stand alone sensor system, the algorithm modeling approach is to be considered for multi-sensor data fusion and state estimate linearization. In system modeling, the study of the environment modeling approach is among the crucial items for the system behavior anticipation and estimation of results in various environmental conditions. The modeling approaches are considered and studied aiming for improved system feedback accuracy [22], [13], [26].

2.2 Navigation Equation

Navigation equations refer to algorithms and mathematical formulas for navigation systems to determine the altitude and attitude of a flying vehicle. The study's concern here is the inertial navigation equations as the fundamental equations for navigation systems. inertial navigation equations rely on angular velocity and acceleration to determine vehicles' orientation and position. Navigation algorithms involve various coordinate frames and the transformation of coordinates between them. For example, inertial sensors measure motion concerning an inertial frame which is resolved in the host platform's body frame. This information is further transformed into a navigation frame. A global positioning system (GPS) receiver initially estimates the position and velocity of the satellite in an inertial orbital frame. Since the user wants the navigational information with respect to the Earth, the satellite's position and velocity are transformed to an appropriate Earth-fixed frame. Since measured quantities are required to be transformed between various reference frames during the solution of navigation equations, it is important to know about the reference frames and the transformation of coordinates between them [22], [26], [12]. İnertial navigation equations for flying vehicles are categorized into acceleration and angular velocities since the vehicle involves motion. And also the Eulers equation for the orientation of the vehicle. This Euler equation depends on the translation and transformation matrices due to the yaw, pitch, and roll of the flying vehicle. Considering rotation between two frames, the general rotation matrix is C[1].

$$C_b^n = \begin{bmatrix} \mathrm{cs}\,\theta\,\mathrm{cs}\,\psi & \mathrm{sn}\,\phi\,\mathrm{sn}\,\theta\,\mathrm{cs}\,\psi - \mathrm{cs}\,\phi\,\mathrm{sn}\,\psi & \mathrm{sn}\,\phi\,\mathrm{sn}\,\psi + \mathrm{cs}\,\phi\,\mathrm{sn}\,\theta\,\mathrm{cs}\,\psi \\ \mathrm{cs}\,\theta\,\mathrm{sn}\,\psi & \mathrm{cs}\,\phi\,\mathrm{cs}\,\psi + \mathrm{sn}\,\phi\,\mathrm{sn}\,\theta\,\mathrm{sn}\,\psi & \mathrm{cs}\,\phi\,\mathrm{sn}\,\theta\,\mathrm{sn}\,\psi - \mathrm{sn}\,\phi\,\mathrm{cs}\,\psi \\ -\sin\theta & \mathrm{sn}\,\phi\,\mathrm{cs}\,\theta & \mathrm{cs}\,\phi\,\mathrm{cs}\,\theta \end{bmatrix} \tag{2.1}$$

Where cs, sn, $\psi, \theta, and\ \phi$ are cosine, sine, yaw, pitch, and roll angles respectively. C_b^n is the rotation matrix of the body relative to the navigation frame. The rotation matrix of the navigation frame relative to the body frame is given by $C_n^b = (C_b^n)'$

The derivation Euler angles are calculated directly from the direction cosine matrix. The below formulas do not apply to an angle 90^o pitch.

$$\begin{aligned} \psi &= \arctan\left[\frac{C_{21}}{C_{11}}\right] \\ \theta &= \arcsin[-C_{31}] \\ \phi &= arctan\left[\frac{C_{32}}{C_{33}}\right] \end{aligned} \tag{2.2}$$

Taking into account the latitudes, longitude, and altitude, calculating the position vector is possible [27].

$$r^e = \begin{bmatrix} (N+h)cos\varphi cos\lambda \\ (N+h)cos\varphi sin\lambda \\ (N(1-e^2)+h)sin\varphi \end{bmatrix} \tag{2.3}$$

Where r^e =(xe,ye, ze) is the coordinate of the position vector in the earth frame. φ is latitude, λ is longtude and $h\ is\ altitude.$ Knowing latitude at h=0, the below equations are a simple way to use in analytically find the latitude, longitude, and altitude hence easy to know the position of an object.

Lattitude φ_0=$\tan^{-1}(\frac{\mathrm{ze}}{\sqrt{x_e^2+y_e^2}}(\frac{1}{1-e^2}))$ at h=0

$$\begin{bmatrix}\varphi\\ \lambda\\ h\end{bmatrix} = \begin{bmatrix}\tan^{-1}\left(\frac{\mathrm{ze}}{\sqrt{x_e^2+y_e^2}}\left(1+\frac{e^2 N sin\varsigma_0}{\mathrm{ze}}\right)\right)\\ \tan^{-1}\frac{y_e}{x_e}\\ \frac{\sqrt{x_e^2+y_e^2}}{cos\varsigma_0}-N\end{bmatrix} \tag{2.4}$$

where eccentricity e=$\sqrt{2f-f^2}$ and flattening $f=\frac{R_e-R_p}{R_e}$, R_e *and* R_p *are equatorial radius and polar radius of the earth respectively.* The rotation matrix of the earth frame relative to the navigation frame is denoted by

$$C_e^n = \begin{bmatrix}-cos\lambda sin\varphi & -sin\varphi sin\lambda & cos\varphi\\ -sin\lambda & cos\lambda & 0\\ -cos\lambda cos\varphi & -cos\varphi sin\lambda & -sin\varphi\end{bmatrix} \tag{2.5}$$

then the rotation matrix of the navigation frame relative to earth frame $C_n^e = (C_e^n)'$.

İn the determination of the flying vehicles' orientation and position, the angular velocity is to be considered. the angular velocity is denoted by omega (ω). The angular velocity of the navigation frame with respect to the earth frame is denoted by

$$\omega_{en}^{\ n} = \begin{bmatrix}\dot{\lambda}cos\varphi\\ \dot{\varphi}\\ -\dot{\lambda}sin\varphi\end{bmatrix} \tag{2.6}$$

The real general navigation equations are denoted by and *where* $\omega_{nb}^b = \omega_{ib}^b$- $C_b^n\omega_{nb}^n$ ω_{ib}^b is the output of gyroscope measurement readings. The angular velocity of a body relative to the navigation frame has three independent equations that can be solved as $\dot{\Theta}$=E(Θ) ω_{nb}^b *for* $\Theta = \begin{bmatrix}\phi\\ \theta\\ \psi\end{bmatrix}$ where $\dot{\Theta}$ is the Euler angular rates and Θ is Euler's angles (roll, pitch, yaw) that is 123 series. at t=0

$$\begin{aligned}\dot{v}^n &= C_b^n f^b + g^n - (\omega_{in}^n + 2\omega_{ie}^n)v^n \\ f^b &= C_n^b[\dot{v}^n - g^n + (\omega_{en}^n + 2\omega_{ie}^n)v^n]\end{aligned} \tag{2.7}$$

where $\omega_{ie}^{n} = \begin{bmatrix} 0 \\ 0 \\ \omega_e \end{bmatrix}$

The position rate estimation is denoted by

$$\dot{r} = Dv^n \tag{2.8}$$

$$\omega_{nb}^{b} = \omega_{ib}^{b} - C_n^b \omega_{in}^{n}$$

$$D = \begin{bmatrix} \frac{1}{R+h} & 0 & 0 \\ 0 & \frac{1}{R+h} & 0 \\ 0 & 0 & -1 \end{bmatrix}$$

The vehicle state estimate is denoted by $\dot{x}$=$f(x,u)$. Where $x = \begin{bmatrix} \Theta \\ v^n \\ P \end{bmatrix}$and $u = \begin{bmatrix} f^b \\ \omega_b \end{bmatrix}$

P= $\begin{bmatrix} x \\ y \\ z \end{bmatrix}$, $\Theta = \begin{bmatrix} \phi \\ \theta \\ \psi \end{bmatrix}$, $v^n = \begin{bmatrix} v_n \\ v_e \\ v_d \end{bmatrix}$, $f^b = \begin{bmatrix} f_x \\ f_y \\ f_z \end{bmatrix}$, $\dot{r} = \begin{bmatrix} \dot{\varphi} \\ \dot{\lambda} \\ \dot{h} \end{bmatrix}$,and $\omega_b = \begin{bmatrix} \omega_x \\ \omega_y \\ \omega_z \end{bmatrix}$

Accurate position, orientation, and translation of flying vehicles result in a safe flight navigation system which is the major item necessary for flying vehicles.

2.3 INS Discretization

To calculate the vehicle's attitude, velocity, and position, the INS mechanization uses the inertial dynamic equation of mechanization. The four coordinate frame scripts are used. These are n- for navigation frame, e- for earth frame, b- for body frame, and i- for inertial frame (Wu, 2021).

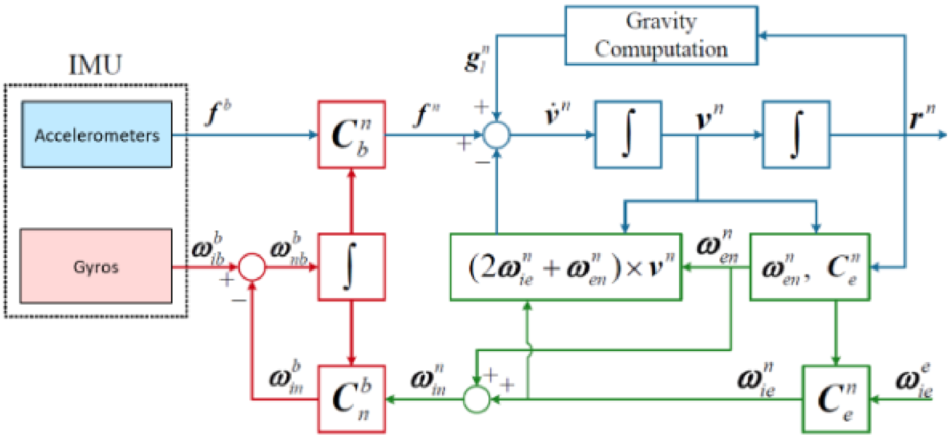

Figure 2 2. INS block diagram (Young Yoon Jang 6 July 2020)

When the IMU is installed on the vehicle incorporated with KF dynamic readings. Noise covariance estimation algorithm for INS /GNSS integrated navigation-based.

The KF measurement vector is the difference in velocity between the GNSS observation and the INS prediction.

Based on the real state estimation system of the INS model.

$$\dot{x} = f(x, u, w) \tag{1}$$

Where $\dot{x}$, x, u, w represent continuous real state space estimation, state vector, real system input vector, and system sensor noise respectively. The state vector is composed of position, velocity, and orientation vectors, u is the input vector for the accelerometer and gyroscope readings and f is a nonlinear function describing the dynamic system.

In this context of an Inertial Navigation System (INS), discretization refers to the process of transforming continuous-time INS models into discrete-time models that may be used with digital computers. For real-time control and navigation applications, this is essential. To estimate location, velocity, and orientation, the method involves discretizing the state-space representation of the INS dynamics. Typically, this involves integrating accelerations and angular rates [1], [26].

The state vector x_k, which normally consists of position, velocity, and orientation, is estimated by an INS using data from accelerometers and gyroscopes. The depiction of state-space in continuous time as:

$$x_k = F(x_{k-1}, u_{k-1}, w_{k-1}) \tag{2}$$

To discretize the time continuous model, the approximation of the state evolution over discrete time steps.the discrete definition of time points Δt.

Dynamic state discretization at the time step can be approximated using numerical integration methods which could be either the Euler method or the range Kutta method.

Euler discretization method

$$x_k = x_{k-1} + \Delta t f(x_{k-1}, u_{k-1}, w_{k-1}) \tag{3}$$

Range Kutta method:

$$k_1 = f(x_{k-1}, u_{k-1}, w_{k-1})$$

$$k_2 = f(x_{k-1} + \tfrac{\Delta t}{2} k_1, u_{k-1}, w_{k-1}) \tag{2.13}$$

$$k_3 = f(x_{k-1} + \frac{\Delta t}{2} k_2, u_{k-1}, w_{k-1})$$

$$k_4 = f(x_{k-1} + \Delta t k_3, u_{k-1}, w_{k-1})$$

Therefore the general form is

$$x_k = x_{k-1} + \frac{\Delta t}{6} f(k_1 + 2k_2 + 2k_3 + k_4)$$

$$x_{k-1} + \frac{\Delta t}{6} f(k_1 + 2k_2 + 2k_3 + k_4) = F(x_{k-1}, u_{k-1}, w_{k-1})$$

$$x_k = F(x_{k-1}, u_{k-1}, w_{k-1}) \tag{4}$$

The INS measurement discretization involves measurement updates

$$z_k = H_k x_k + v_k \tag{5}$$

Where z_k, H_k, x_k, *and* v_k are the measurement vector, the measurement matrix, the INS prediction result at time k from the navigation, and the measurement zero-mean Gaussian noise respectively.

Due to the double integration of accelerometer measurements to obtain location and the integration of gyroscope measurements to obtain orientation, the fundamental difficulty with an INS is that small sensor errors can accumulate and worsen over time. Covariance analysis and state-space models can be used to examine how these errors spread.

Relative navigation errors from Inertial Navigation Systems (INS) can be modeled to see how they affect navigation accuracy.

2.4 Inertial navigation system errors

Inertial Navigation Systems (INS) are widely used in relative navigation systems due to their ability to provide continuous and independent position, velocity, and orientation information. However, INS are subject to various errors that can accumulate over time and degrade the accuracy of the navigation solution. Some of the errors, are:

Sensor error s which could be a result of gyroscope and accelerometer bias, scale factor. The constant offset may cause orientation, velocity, and position errors.

Alignment error involves inertial misalignment and drift errors in the initial alignment of the INS with the reference frame. This includes errors in the initial position, velocity, and orientation and gradual change in alignment over time due to sensor biases and other errors.

Environmental errors occur due to the temperature effects leading to drift, bias, and magnetic interference in the case of the system with the magnetometer. And the additional INS error due to the integrated systems is an integration error.

Mechanization errors arise from incorrect compensation for the Coriolis and centripetal forces in the mechanization equations [24], [1], [18].

The accelerometers and gyroscopes and their gradual integration are the main causes of these inaccuracies. The difference between the real estimated state and the nominal state estimation analyzes the error state vector.

$$\dot{x}^n = f(x_n, u_n)$$
$$\dot{x} = f(x, \tilde{u})$$
$$\tilde{u} = u - w \tag{2.16}$$

Where $\dot{x_n}$ and $\dot{x}$ are nominal and real system state estimates. $\tilde{u}$, u and w are real measured inertial measurement unit (IMU) measured output, real IMU input, and IMU noise respectively.

by linearizing the state space equation to the nominal state, the error state equations at time step k are obtained as

$$\Delta\dot{x} = \dot{x} - \dot{x}_n$$
$$\Delta\dot{x} = f(x_n, u_n) + \frac{\partial f}{\partial x}\Delta x + \frac{\partial f}{\partial u}\Delta u - f(x_n, u_n) \tag{6}$$

For the above differential equation $x = x_n$ and $u = u_n$.

$$\Delta\dot{x} = A\Delta x + Bw\ ,\ A = \frac{\partial f}{\partial x}\Big|_{\substack{x=x_n\\ u=u_n}},\ \ B = \frac{\partial f}{\partial u}\Big|_{\substack{x=x_n\\ u=u_n}}$$

The above equation can be discretized as:

$$\Delta x_k = F\Delta x_{k-1} + Gw_{k-1} \tag{7}$$
$$F = e^{A\Delta t}, \qquad G = \left(\Delta t I + \frac{\Delta t^2}{2}A + \frac{\Delta t^3}{3!}\ A^2 + \cdots + \frac{\Delta t^n}{n!}A^{n-1} + \cdots\right)B$$

The covariance matrix error P_k propagation can be done by flowwing equation

$$P_k = FP_{k-1}F^T + GQ_{k-1}G^T \tag{8}$$

where:

F_k is the state transition matrix obtained from the linearized error state model and Q_{k-1} is the process noise covariance matrix of w_{k-1}.

The state transition matrix F depends on the system dynamics and the errors being modeled. The process noise covariance matrix Q_K accounts for the sensor noise and biases.

Based on the signal distortion and errors generated when using INS and INS/GPS integrations for relative navigation systems due to systematic and environmental factors, system calibration methods are to be taken into account for the reliable system output by calibrating system sensors and the development of the visual algorithm by integrating distance sensor cameras using IMU and Kalman filter is expected to be a solution mostly at low altitudes of flying vehicle approaching to land.

CHAPTER 3

VISUAL NAVIGATION

The camera plays a crucial role in computer vision by enabling us to capture the world around us and utilize the resulting images for a wide range of applications. Vision-based navigation is anticipated to serve as a practical navigation solution for relative navigation systems in aerial vehicles. Stereo cameras can be used for terrain mapping, visual odometry, and landmark recognition, among other applications that require the acquisition of comprehensive visual information about the surrounding environment. This data richness enables more dependable and accurate navigation. The pinhole model, which outlines the mathematical representation of projecting points in three dimensions onto an image plane, serves as the foundational camera model. This model is represented as the pinhole at which light rays pass through to form an image on the camera sensor [21].

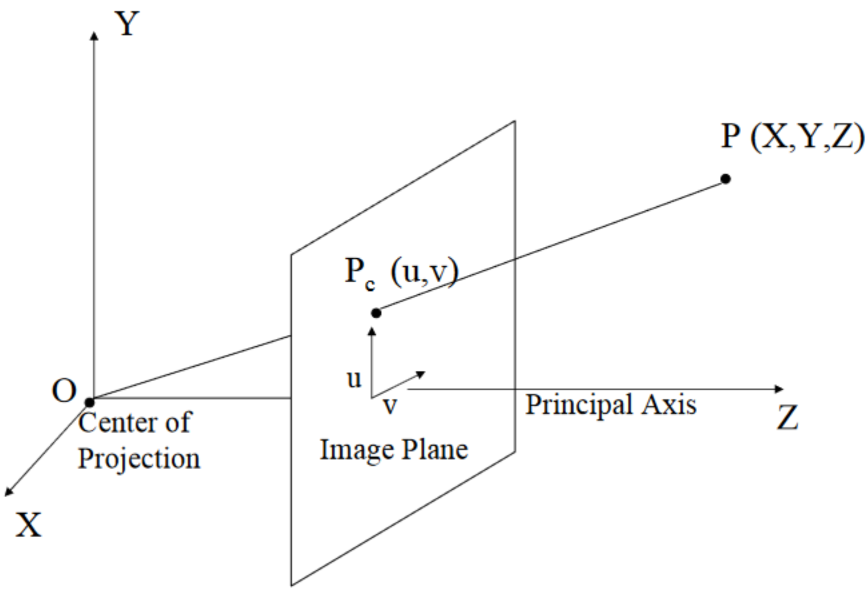

Figure 3 1**.** Pinhole model (Hartley and Zisserman, 2003)

The figure 3.1 shows a pinhole camera model on how camera image is formed. Taking a camera with its major axis parallel to the Z axis and its center of projection

O is seen in the above figure. Since the image plane is at focus, the focal length f is separated from O. On the image plane of the camera, a 3D point P = (X, Y, Z) is photographed at coordinate

P_c = (u, v). The camera calibration matrix C, which converts 3D P to 2D P_c, will be located first. Similar triangles can be used to find Pc, as we have already demonstrated.

$$\frac{f}{Z} = \frac{u}{X} = \frac{v}{Y} \tag{9}$$

From this equation the projection image points

$$u = \frac{Xf}{Z}$$
$$v = \frac{fY}{Z} \tag{10}$$

Translation of Pc to the desired origin is required if the Z-axis intersection of the image plane and the origin of the 2D image coordinates system do not line up. Give (c_x, c_y) the definition for this translation. Therefore, at this moment (u, v) is

$$u = \frac{Xf}{Z} + c_x$$
$$v = \frac{fY}{Z} + c_y \tag{11}$$

When considering homogeneity equations (39) and (40) can be expressed as

$$\begin{bmatrix} u \\ v \\ w \end{bmatrix} = \begin{bmatrix} f & 0 & c_x \\ 0 & f & c_y \\ 0 & 0 & 1 \end{bmatrix} \begin{bmatrix} X \\ Y \\ Z \end{bmatrix} \tag{12}$$

In both the u and v directions of the camera image coordinates, the resolution will be the same if the pixels are square. Nonetheless, we consider rectangle pixels with resolutions of u and m_v pixels in the u and v directions, respectively, for a more generic scenario. Thus, the u and v coordinates of P_c should be multiplied by m_u and m_v, respectively, to measure it in pixels [21]. Therefore the equations

$$u = \frac{Xf}{Z} + m_u c_x$$
$$v = \frac{fY}{Z} + m_v c_y \tag{13}$$

$$\begin{bmatrix} u \\ v \\ w \end{bmatrix} = \begin{bmatrix} fm_u & 0 & m_u c_x \\ 0 & fm_v & m_v c_y \\ 0 & 0 & 1 \end{bmatrix} \begin{bmatrix} X \\ Y \\ Z \end{bmatrix} \tag{14}$$

$\alpha_x = fm_u, \alpha_y = fm_v, p_x = m_u c_x \; and \; p_y = m_v c_y$

Then the equation is expressed as

$$\begin{bmatrix} u \\ v \\ w \end{bmatrix} = \begin{bmatrix} \alpha_x & 0 & p_x \\ 0 & \alpha_y & p_y \\ 0 & 0 & 1 \end{bmatrix} \begin{bmatrix} X \\ Y \\ Z \end{bmatrix} \tag{15}$$

From P= $\begin{bmatrix} X \\ Y \\ Z \end{bmatrix}$ and K= $\begin{bmatrix} \alpha_x & 0 & p_x \\ 0 & \alpha_y & p_y \\ 0 & 0 & 1 \end{bmatrix}$,

$$\begin{bmatrix} u \\ v \\ w \end{bmatrix} = KP \tag{16}$$

Where K is the intrinsic parameters of the camera (pixel, focal length).

K= $\begin{bmatrix} \alpha_x & s & p_x \\ 0 & \alpha_y & p_y \\ 0 & 0 & 1 \end{bmatrix}$ when it has skew parameters.

This typically occurs when the axes that coordinate the image, u and v, are not orthogonal to one another. It should be noted that K is a 3 × 3 upper triangular matrix. This is typically referred to as the camera's intrinsic parameter matrix.

To align the camera coordinate system with the setup shown in Figure 1, we must perform a rotation and translation if the camera's center of projection is not at (0, 0, 0) and z is not perpendicular to the image plane. Let T (T_x, T_y, T_z) represent the camera translation vector to the XYZ coordinate origin. Allow the rotation to be represented by a 3 × 3 rotation matrix R to align the primary and Z axes. The 3 × 4 matrix is the result of applying translation and rotation in order to generate the matrix [10], [28].

The rotation matrix R which represents $R_x, R_y, and\ R_z$ matrices.

$$R_x = \begin{bmatrix} 1 & 0 & 0 \\ 0 & \cos\alpha & sin\alpha \\ 0 & -sin\alpha & \cos\alpha \end{bmatrix}$$

$$R_y = \begin{bmatrix} \cos\beta & 0 & sin\beta \\ 0 & 1 & 0 \\ -sin\beta & 0 & \cos\beta \end{bmatrix} \qquad (3.10)$$

$$R_z = \begin{bmatrix} \cos\theta & sin\theta & 0 \\ -sin\theta & \cos\theta & 0 \\ 0 & 0 & 1 \end{bmatrix}$$

Where α, β, and θ are the rotation angles in the x,y, and z directions. In flying vehicles, these angles represent roll, pitch, and yaw.

The extrinsic parameter matrix is

$$E = [R \quad RT] \qquad (3.11)$$

The camera transformation matrix is expressed by

$$\mathrm{K}[R \quad RT] \qquad (17)$$

Here the camera projection points is

$$P_C = \mathrm{K}[R \quad RT] \qquad (3.13)$$

The camera calibration matrix C is

$$C = \mathrm{K}[R \quad RT] = KR[I \quad T] \qquad (18)$$

Therefore $P_C = CP$

3.1 Visual Navigation With Stereo Cameras

Navigation with stereo cameras involves two synchronized cameras with a known baseline to capture image points from different viewpoints. This allows the 3D depth perception environment reconstructions. The method of stereo camera-based navigation improves the ability of flying vehicles to detect obstacles and estimate the vehicles' position and velocity relative to the known platform [3], [29][30].

Assuming that the two cameras' optical sensors are coplanar and have the same characteristics and parameters the stereo processing is achieved as shown below:

3.1.1 Stereo camera processing

Taking world points P=[X, Y, Z] projected into stereo cameras the projection points are identified $P_{c1} = [x, y]$ and $P_{c2} = [x', y']$ focusing at the same image point [30].

Knowing the baseline (b) between two cameras, and the image disparity (d) due to the two camera images, the altitude is determined by triangulation.

$$Z = \frac{fb}{d} \tag{3.15}$$

Where f is the camera pixel and disparity d = $|x - x'|$

Matching points by stereo cameras method obtain disparity. The position centers can be determined using the center coordinates. To measure the duration between frames, the speed computation makes use of the location centers to calculate the distance between nearby frame centers. All the object points are estimated to be approximately at the same distance from each camera. The extraction and object size is estimated when disparity detection is performed.

Obtaining the rest of the image points are computed by

$$X = \frac{xZ}{f}, Y = \frac{yZ}{f} \tag{3.16}$$

Projecting 3D world coordinates to 2D image points is denoted by normalizing Z-axis points.

$$x = \frac{fX}{Z}, y = \frac{fY}{Z} \tag{3.17}$$

The three-dimensional homogenous expression by taking camera reference when disparity is obtainable and is denoted by

$$P_c = (X, \quad Y, \quad Z, 1)^{T} \tag{19}$$

This represents the transformation of world point to camera points when disparity is possible to be obtained. The matrix to convert 3D points from the local reference system of each camera to the world points centered in a pattern is determined by extrinsic parameters from each camera of the stereo camera system.

3.1.2 Stereo Camera Feature Detection

Stereo cameras are used in the visual navigation of flying vehicles to determine depth perception and feature detection by the triangulation principle. This principle is done by capturing the images using stereo cameras from different two viewpoints to determine object position and feature detection. Feature detection refers to the areal point justification in the reliable scene identified in both stereo cameras. Scale-invariant transform (SIFT) and speed-up robust features (SURF) are the popular feature detection algorithms in visual navigation systems [2], [3].

The detection of features by the SIFT involves some parts that include scale-space extrema detection, keypoint localization, orientation assignment, and keypoint descriptor.

Scale-space extrema detection (SSED) is to detect and identify the most reliable points that are invariant to scale. It detects key points by searching for the local extrema difference of Gaussian [4], [5].

The original image point of scale space representation $I(x, y)$ is Gaussian convolved of a different scale (σ) sigma to make blurred image series.

$$L(x, y, \sigma) = G(x, y, \sigma)I(x, y)$$
$$G(x, y, \sigma) = \frac{1}{2\pi\sigma^2} e^{\frac{-x^2+y^2}{2\sigma^2}} \quad (3.19)$$

The difference of Gaussian function convolved with the image, $D(x, y, \sigma)$ can be calculated from the difference of two closest scales separated by a multiplicative constant factor k. This allows the efficient detection of stable positions of key points in space scale [4], [5].

$$D(x, y, \sigma) = \big(G(x, y, k\sigma) - G(x, y, \sigma)\big)I(x, y)$$

$$D(x, y, \sigma) = L(x, y, k\sigma) - L(x, y, \sigma) \tag{3.20}$$

Where k is the scale factor constant and $D(x, y, \sigma)$ is the local extrema.

The keypoint localization is identified as local extrema in the difference of Gaussian.

Tylor expression of DoG

$$D(x) = D + \frac{\partial D^T}{\partial x}x + \frac{1}{2}x^T\frac{\partial^2 D}{\partial x^2}x \tag{3.21}$$

Where $x = (x, y, \sigma)^T$ is the detected keypoint offset, D is the difference of Gaussian, $\frac{\partial D}{\partial x}$ is gradient of D, and $\frac{\partial^2 D}{\partial x^2}$ is Hessian matrix.

The localization of x is done where $D(x)$ has reached an extremum and x is iteratively refined.

This makes the involvement of each point comparison in the scale space.

Orientation key points: The orientation to each key point based on the local image for each key point was calculated using pixel differences as [5]

$$m(x, y) = \sqrt{(L(x+1, y) - L(x-1, y))^2 + (L(x, y+1) - L(x, y-1))^2}$$

$$\theta(x, y) = tan^{-1}\left(\frac{L(x,y+1) - L(x,y-1)}{L(x+1,y) - L(x-1,y)}\right) \tag{3.21}$$

Where $\theta(x, y)$ and $m(x, y)$ are orientation gradents assignment feature detection using the SIFT technique.

The process of detecting features in SIFT starts with generating a scale space representation using Gaussian blurring, identification of key points as local extrema in the difference of Gaussian pyramid, and then giving the key points orientations based on gradient orientation, generation of descriptor for each key point and matching the descriptors for 3D image reconstruction and recognition. The orientation gradient and descriptor coordinates are rotated with respect to the keypoint orientation in order to ensure invariance orientation.

SIFT makes a descriptor by including the orientation and gradient with in neighborhound arround the main target. To perfprm this, vector decriptor $V(x, \sigma)$ is calculated from the orientation gradient weighed by their position and magnitudes.

$$V(x, \sigma) = [\sum_P w(P - x, \sigma) P\, e^{-\frac{||P-x||^2}{2\sigma^2}} \quad (3.22)$$

P represents local neighborhood points, $w(P - x, \sigma)$ is the weight function, and σ is the scale to where descriptor is calculated.

The discriptor matching with SIFT , uses Euclidian distance to measure descriptors similarities.

$$D(V_1, V_2) = \sqrt{\sum_i (V_{1i} - V_{2i})^2} \quad (3.23)$$

The key matching process involves the Euclidian distance between descriptors and SIFT to find the neighborhoods and match the closest matches on a ratio of

$$ratio = \frac{||v_1 - u||}{||v_2 - u||} \quad (3.24)$$

Where $v_1$and v_2 are the closest two descriptors from the second image, u is the descriptor from the first image.

The SIFT technique makes use of the difference of Gaussians, a Laplacian of Gaussian (LoG) approximation. The Gaussian difference is the distance between the Gaussian blurrying of different images. This procedure is carried out for the various image octaves in the Gaussian pyramid.

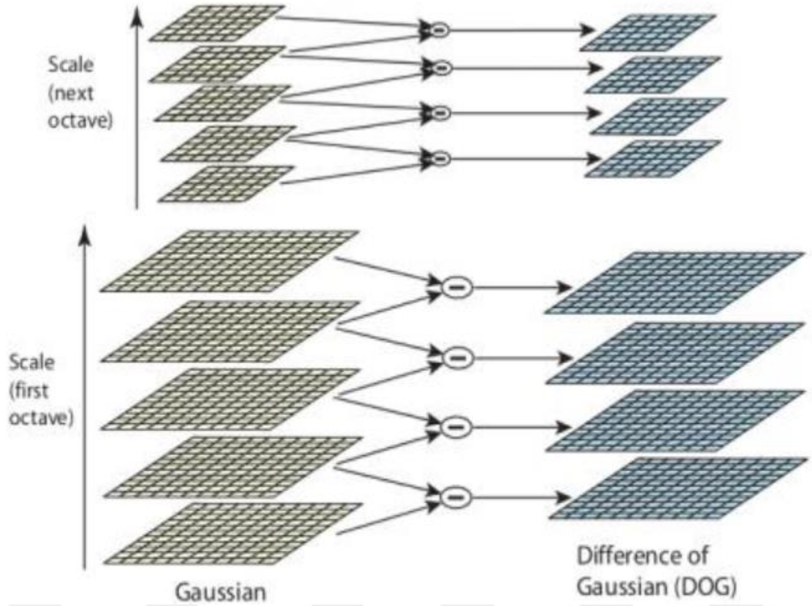

Figure 3 2. Image detection using the SIFT technique
(https://docs.opencv.org/4.x/da/df5/tutorial_py_sift_intro.html 15 july 2024)

The fig 3.2 shows how the feature is detected by SIFT by using difference of Gaussian.

The working principles between SURF and SIFT are the same except that the SURF as the name implies, is faster and more robust to scale changes, and orientation. It uses image integral in speeding up filter calculations and approximates Gaussian derivatives using Haar wavelets.

CHAPTER 4

ESTIMATION METHODS

Modern navigation systems utilize state estimation techniques to efficiently process data from various sensors, advancing navigation and tracking technologies. State estimation methods provide the state estimate based on the available measurements and a known state-space model. According to [16], and [32] the state estimation methods are categorized into exact, local, and global methods. Under which the exact methods have been typically designed for a set of linear models. For this set, the solution to the Bayesian recursive relations (BRRs) results in reproducible conditional probability density functions (PDFs), i.e. the conditional PDFs at subsequent time instants share the same distribution and, thus, recursive conditional PDF computation reduces to recursive computation of conditional PDF parameters only. The exact method is presented by Kalman Filter (KF).

Local methods are based on two approximations; first, the joint conditional predictive state and measurement PDF is assumed to be Gaussian; second, the nonlinear functions are linearizeable. The former approximation results in a linear structure of a local filter with respect to the measurement, and together with the latter approximation, it allows the use of the (linear) KF design technique also for nonlinear models. For this method, the linearisation can be found in derivative-based and derivative-free. Derivative-based involves the extended Kalman filter (EKF).

The global methods provide accurate and consistent estimates in the form of conditional probability density functions (PDFs) without any assumption of the conditional distribution family. Global methods are capable of estimating the state of a non-Gaussian or strongly nonlinear system usually at the cost of higher demand. This method can simultaneously involve an extended Kalman filter (EKF) and/or unscented Kalman filter (UKF) for system linearization of non-linear functions.

State estimation in navigation applications can be either linear or non-linear estimator. The linear estimator deals with the stochastic estimation system whereas the non-linear estimator deals with the various stages of nonlinear stochastic systems. The well-known linear estimator in navigation systems that is to be discussed is the standard/linear Kalman filter (KF). Nonlinear estimator includes Extended Kalman Filter (EKF), Unscented Kalman Filter (UKF), Particle filter (PF), and multiple model adaptive estimator (MMAE). Under which extended Kalman filter is discussed in this study as the system estimator.

4.1 Least Square

The least square method is used when there are many equations than the unknowns. The residual vector's sum of squares is minimized by the solution. Assume that there are n parameters in a vector x wish to estimate from vector z of m measurement noise where m is greater than n [27], [33].

$$z = Hx + v \tag{4.1}$$

Where the matrix $H_{m\times n}$ is a known design matrix.

When estimating vector x using the least squares approach, the sum of the squares of the components of the residual vector z- Hx is minimized and is represented by $\hat{x}$.

Minimize

$$\| \mathrm{z} - H\hat{x} \|_R^2 = (\mathrm{z} - H\hat{x})_{1\times m}^T R^{-1} (\mathrm{z} - H\hat{x}_{1\times m}) \tag{4.2}$$

$$\| \mathrm{z} - H\hat{x} \|_R^2 = z^T R^{-1} z - z^T R^{-1} H\hat{x} - zR^{-1}(H\hat{x})^T + (H\hat{x})^T R^{-1} H\hat{x}$$

Differentiating the equation with respect to the state estimate $\hat{x}$

$$\frac{\partial(\|\mathrm{z}- Hx\|_R^2)}{\partial\hat{x}} = 0 - z^T R^{-1} H - (H^T R^{-1} z)^T + (H^T R^{-1} H\hat{x})^T + \hat{x}^T H^T R^{-1} H \tag{4.3}$$

$$\frac{\partial(\|\mathrm{z}- Hx\|_R^2)}{\partial\hat{x}} = -2(z^T R^{-1} H - \hat{x}^T H^T R^{-1} H)$$

Equating to zero derivatives for the minimization

$$z^T R^{-1} H - \hat{x}^T H^T R^{-1} H = 0$$

$$\hat{x}^T = z^T R^{-1} H (H^T R^{-1} H)^{-1}$$

$$\hat{x} = (H^T R^{-1} H)^{-1} H^T R^{-1} z$$

$$Cov(\hat{x}) = KRK^T \text{ , } K = (H^T R^{-1} H)^{-1} H^T R^{-1} \tag{20}$$

Where R is measurement covariance. Therefore the value of $\hat{x}$ is deduced by differentiating $\| \text{z} - H\hat{x} \|^2$ with respect to $\hat{x}$ state estimate.

4.2 Kalman Filter

The development of the Kalman filter in the 1950s update has impacted the engineering field to more advancements in filtering and state estimations since it is a fundamental state estimate and control system tool that critically plays a big role in various applications including aerospace engineering, robotics, and many others makes it a more reliable tool. Kalman filter is an algorithm that uses a mathematical series of measurements observed with respect to time and results in accurate variable estimates. It generates a statistically optimum estimation of the underlying system state by operating recursively on streams of noisy input data.

Filtering algorithms used for navigation systems of positioning are based on the nonlinear equation of state as well as the measurement equation. They operate in a discrete time. Kalman filter allows to estimation error or state of an object in the kth step based on measurements in the k-1th step. Kalman filters use information about the dynamics of the object system.

Kalman filter is applied for both Gaussian and nonlinear systems. And is categorized in various forms including the Kalman filter (KF) which is a method that is based on recursive Bayesian filtering where the system is assumed to be Gaussian, Extended Kalman filter (EKF) is an extension of KF that deals with nonlinear dynamic systems for linearized dynamic systems, Unscented Kalman filter (UKF) is an extension of EKF operates on the statistical parameters of these models subjected to the non-linear transformations. UKF is based on unscented transform (UT), which converts the state vector into a set of weighted sigma points. These points are then used in algorithms for UKF. The UKF algorithm is a set of equations that are necessary to do prediction, innovation, and correction steps [34][35], [36]

Linear Kalman filter is the particular situation that allows the entire statistics of the probability density functions (pdfs) of interest to be expressed as a mean vector and covariance matrix, a unique property that is exploited by the linear Kalman filter. The linear Kalman filter consists of two distinct steps which are propagation of the mean and covariance between time and incorporation of a discrete observation. Under these conditions, the a posteriori pdf is guaranteed to be Gaussian.

The system to be estimated in its steps is represented in terms of a state-space model comprising two equations which are categorized into a state transition equation and observation equation.

State transition equation:

$$\begin{aligned} &x_k = F_k x_k + G_k w_k, \text{ linear form} \\ &F_k = \frac{\partial f}{\partial x}\Big|_{\substack{w=0 \\ x=\hat{x}_{k-1}}}, G_k = \frac{\partial f}{\partial w}\Big|_{\substack{w=0 \\ x=\hat{x}_{k-1}}}, \end{aligned} \tag{21}$$

Observation equation:

$$\begin{aligned} &z_k = H_k x_k + v_k. \text{ Linear form} \\ &E(v) = 0, E(vv^t) = R \end{aligned} \tag{22}$$

Where x_k is the state at time step $[k]$, F_k is the state transition matrix, G_k is the disturbance matrix, w_k is the process noise (assumed to be Gaussian with covariance matrix Q_K), z_k is the observation at time step $[k]$, H_k is the observation matrix, $v_k$is the observation noise (assumed to be Gaussian with covariance matrix R_k)

After having the state space equations, the second filtering algorithm is to predict the next state which is predicted using two equations which are prediction equation and error prediction equation.

State prediction equation:

$$\hat{x}_k^{-} = F_k \hat{x}_{k-1} + B_k u_k \tag{23}$$

Error covariance prediction:

$$P_k^{-} = F_k P_{k-1} F_k^T + Q_k \tag{24}$$

After the prediction step, the system correction and update are necessary. İn doing the system update, kalman gain is the critical factor in order to minimize the system errors. The below equations are used in the system correction and update step.

Kalman gain:

$$K_k = P_k^{-} H_k^T (H_k \, . \, P_k^{-} \, H_k^T + R_k)^{-1} \tag{25}$$

State update estimation:

$$\hat{x}_k = \hat{x}_k^{-} + K_k (z_k - H_k \, \hat{x}_k^{-}) \tag{26}$$

Covariance error update:

$$P_k = (\mathrm{I} - K_k \; H_k) \, P_k^{-} \tag{27}$$

While many systems are well-modeled by linear stochastic equations, most real-world applications are nonlinear at some level. There are many types of nonlinearities to consider. Some examples include non-Gaussian noise sources, saturation effects, nonlinear dynamics or measurement models, and jump discontinuities. All of these effects ultimately result in the true conditional state pdfs being non-Gaussian in nature, which violates the fundamental assumptions of the linear Kalman filter those are the effects of nonlinearities on the linear Kalman filter (KF) (Veth)[17], [36].

4.3 Extended Kalman Filter (EKF)

Acceptable results can be obtained with the extended Kalman filter (EKF) if the degree of nonlinearities is nearly minimal. The system and measurement models are linearized using a first-order Taylor series expansion to form the foundation of the EKF filter design[17], [37].

The EKF extends the Kalman filter to handle nonlinear system dynamics and measurement functions by linearizing them around the current estimate of the state [16], [32]. The state estimate and covariance matrix are updated using prediction and updating steps under the following functions:

Prediction step:

$$\begin{aligned} \hat{x}_k &= f(\hat{x}_{k-1}, u_k, 0) \\ P_k &= F_k P_{k-1} {F_k}^T + Q \\ F_k &= \frac{\partial f}{\partial x} \Big|_{\substack{w=0 \\ x=\hat{x}_{k-1}}} \end{aligned} \tag{28}$$

Measurement

$z_k = h x_k + v_k)$

$H = \frac{\partial h(x)}{\partial x} \Big|_{\hat{x}_{k-1}}$

Update step:

$$\begin{aligned} K_k &= P_k H^T (H P_k H^T + R)^{-1} \\ \hat{x}_k &= \hat{x}_{k-1} + K_k (z_k - h(\hat{x}_{k-1})) \\ P_k &= (I - K_k H) P_{k-1} \end{aligned} \tag{4.13}$$

Where, $f(\hat{x}_{k-1}, u_k)$ is the nonlinear state transition function, F_k is the Jacobian matrix of the state transition function $h(\hat{x}_k)$, $\hat{x}_k$ is state update, P_k is coveriance update, $\hat{x}_{k-1}$ is predictated state, P_k is predicted covariance.

Although the EKF is very widely used in navigation applications

First, the EKF is subject to linearization errors. These linearization errors result in incorrect state estimates and covariance estimates and can lead to unstable operation, known as filter divergence. EKFs can be extremely sensitive to this effect during periods of relatively high state uncertainty such as initialization and start-up. The second issue is the inherently unimodal assumption of the EKF. In cases where multi-modal densities are known to exist, the EKF would not be a good choice (Veth)[17].

CHAPTER 5

CALIBRATIONS

Accurate sensor data is essential for reliable navigation obstacle avoidance and environmental mapping in the world especially for flying vehicles. The sensors provide data required to comprehend the environment around the flying vehicle. Nevertheless, accurate calibration is crucial to guarantee that the information from sensors is accurate and reliable. Sensor calibration is the process of matching sensor readings complying with the standards by modifying the outputs and inaccuracies due to systematic and environmental errors. Such errors include sensor bias, misalignment, scale factor, and signal distortion due to other signal sources.

Various sensor calibration methods are required for the sensor to provide accurate outputs. Single-point calibration and multi-point calibration are the basic ways of sensor calibrations where calibration is performed referring to known standard point and dynamic calibration is another way of calibration that deals with the calibration of dynamic parameters like angular velocities.

5.1 IMU Calıbratıon

The inertial measurement unit model is categorized into accelerometer and gyroscope model. All the errors and calibrations are based on both the gyroscope and accelerometer. Accelerometer and gyroscope measurements can be illustrated mathematically as

$$\begin{aligned} \boldsymbol{f_r} &= \boldsymbol{S_a a + b_a} \\ \boldsymbol{\omega_r} &= \boldsymbol{S_g g + b_g} \end{aligned} \tag{29}$$

Where $\boldsymbol{f_r}$, $\boldsymbol{S_a}$, $\boldsymbol{a}$, $\boldsymbol{b_a}$, $\boldsymbol{\omega_r}$, $\boldsymbol{S_g}$, $\boldsymbol{g}$, ***and*** $\boldsymbol{b_g}$ are raw acceleration measurement, acceleration scale factor, true acceleration vector, acceleration bais, raw gyroscope measurement, gyroscope scale factor, true gyroscope angular vector, and gyroscope bias. The inertial measurement unit calibration procedure is done by reduction of bais, misalignment, and dynamic errors.

Bias calibration for acceleration is done by placing an IMU in a static known position and orientation. Knowing the static position means the true acceleration vector is known and by measuring the raw acceleration, the acceleration bias is computed as:

$$b_a = f_r - a \tag{5.2}$$

IMU calibration is to be done based on the dynamic calibrations due to the angular velocities measured by a gyroscope. The gyroscope measures rotation series at known angular velocities. For the complete calibration, computation of scale factor and misalignment calibration is achieved by using multiple known orientations.

$$\boldsymbol{A_r} = \boldsymbol{S_a A} + \boldsymbol{B_a} \tag{30}$$

where $\boldsymbol{A_r}$ is the matrix of raw measurements, A is the matrix of true values, and $\boldsymbol{B_a}$ is the matrix of biases. Using the least square method solves the scale factor and misalignment issues.

$$\boldsymbol{S_a} = (\,\boldsymbol{A}\boldsymbol{A^T})^{-\boldsymbol{1}}\boldsymbol{A}\boldsymbol{A_r}^{\boldsymbol{T}} \tag{5.4}$$

5.2 Camera Calibration

The extraction of precise and trustworthy 3D metric information from photos requires accurate camera calibration and orientation techniques. If the primary distance, principal point offset, and lens distortion parameters are known, the camera is said to be calibrated. Only the focal length is recovered in many applications, particularly in computer vision, but all of the calibration parameters are typically used for accurate photogrammetric measurements. Photogrammetric measurement has always required camera calibration, and in the modern day, self-calibration is a crucial and frequently used process within photogrammetric triangulation, particularly in high-accuracy close-range measurement. However, there are numerous scenarios where the topology of the image network will not permit robust recovery of camera parameters by on-the-job calibration, despite the extremely rapid development in the adoption of off-the-shelf digital cameras for a variety of novel 3D measurement applications. The calibration of each of these geometric sensors can be decomposed into internal calibration parameters and external parameters. The external calibration parameters are the position and orientation of the sensor relative to some fiducial coordinate system. The internal parameters, such as the calibration matrix of a camera, affect how the sensor samples the scene. [19], [20].

The usual pinhole model can describe a camera. A projection from the world coordinates $P = [X, Y, Z]^T$ to the image coordinates $P = [u, v]^T$ can be represented

As

$$
\begin{aligned}
&P \cong K(RP + t) \\
&K = \begin{bmatrix} f_x & 0 & c_x \\ 0 & f_y & c_y \\ 0 & 0 & 1 \end{bmatrix} \\
&R = \begin{bmatrix} r11 & r12 & r13 \\ r21 & r22 & r23 \\ r31 & r32 & r33 \end{bmatrix}
\end{aligned}
\tag{5.4}
$$

where f_x, f_y, c_x, and c_y are focal lengths and coordinates of principal points in (x, y) direction respectively.

where t is a 3-vector representing the camera's position, R is a 3 × 3 orthonormal matrix reflecting the camera's orientation, and K is the intrinsic matrix of the camera. Real-world situations may result in noticeable lens distortion on the camera; this can be represented as a 5-vector parameter made up of tangent and radial distortion coefficients

vision-based camera calibration models have traditionally employed reference grids, the calibration matrix K being determined using images of a known object point array pattern

Tsai’s calibration model assumes that some parameters of the camera are provided by the manufacturer, to reduce the initial guess of the estimation. It requires n features points (n > 8) per image and solves the calibration problem with a set of n linear equations based on the radial alignment constraint. A second order radial distortion model is used while no decentring distortion terms are considered. The two-step method can cope with either a single image or multiple images of a 3D or planar calibration grid, but grid point coordinates must be known. (Fraser, 2006).

A planar pattern must be positioned in several orientations in front of the camera for Zhang's calibrating approach to work. The presented technique computes a projective transformation between the image points of the n distinct images, up to a scale factor, using the extracted checkerboard pattern corner points. The camera's interior and exterior parameters are then recovered using a closed-form solution, while the third- and fifth-order radial distortion terms are recovered using a linear least-squares approach. All recovered parameters are refined through a final non-linear minimization of the re-projection error, which is solved using the Levenberg-Marquardt technique. which necessitates at least five views of a planar

Although the ideal Lens cameras do not involve any distortion in camera calibration, real lenses are likely to deviate from the projection rectilinearity. Having a real lens system requires a method that handles distortion in camera calibration

have been working with ideal lenses that are free from any distortion. However, as seen before, real lenses can deviate from rectilinear projection, which requires more advanced methods. This section provides just a brief introduction to handling distortions.

Often, distortions are radially symmetric because of the physical symmetry of the lens.

5.3 Stereo Camera Calibration Using Checkerboard

Traditionally, several existing approaches have consistently employed narrow-angle cameras to capture stereo pictures of black and white checkerboard patterns. Maintaining the pattern close to the stereo cameras is essential to achieve more accurate calibration results. There may be instances where this orientation reduces the amount of possible positions. Sometimes it is impossible to capture the entire region of the checkerboard pattern. The use of wide-angle lenses is one potential fix for this occlusion issue.

The stereo setup may not be able to fully capture images of the checkerboard pattern even if a wide-angle lens is used. We have trouble covering the entire checkerboard pattern at close range because of the stereo setup of a new checkerboard pattern which has been employed in place of the traditional black and white pattern.

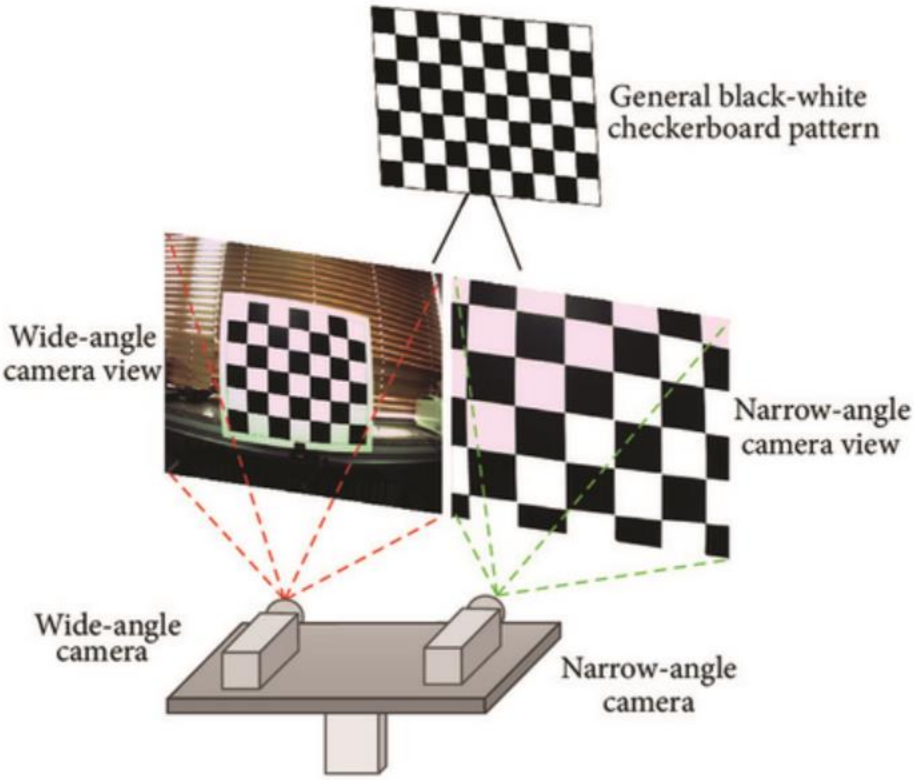

Figure 5 1**:** Checkerboard for stereo camera calibration (Pathum Rathnayaka, Seung-Hae Baek, Soon-Yong Park • Pathum Rathnayaka, Seung-Hae Baek, Soon-Yong Park 2017)

An illustration demonstrating the variation in viewing angles between wide-angle and narrow-angle cameras. A larger coverage of the scene is provided by the wide-angle camera on the left. The narrow-angle camera which may only captures a portion of the image on the right side. The narrow-angle camera shows a portion of the overall checkerboard design.

Wide-angle cameras have significant barrel distortions which is one of the drowbacks. Erroneous matrix calculations may result from stereo calibration that are performed without first addressing distortion. Thus two stereo calibration techniques are by first removing distortions from input wide and narrow-angle images to preserve the inner pattern. While shooting with a narrow lens and the outer pattern when shooting with a wide angle for mono camera calibration wherein separate calibrations are done wide and narrow-angle cameras.

Calibration using two transformation matrices, the wide and narrow angles camera transformation matrices are multiplied in the stereo calibration method. After the cameras have been mono-calibrated independently, simultaneously record stereo image sequences of checkerboard pattern from both cameras. Maintain a close spacing between the cameras and the checkerboard pattern when taking images so that the wide-angle camera can view the entire pattern and the narrow-angle camera can view the entire inner pattern. According to this transformation matrices method, the origin of the initial outer checker pattern is the intersection point of the checkerboard pattern which is used as the global coordinate system. By simply adding the distance between the two origins, the inner pattern origin at the crossing point is relocated toward the outer pattern origin given that the inner and outer patterns are two distinct checkerboards.

5.4 Camera Calibration With Respect to IMU

Aligning the coordinate systems of both the camera and the Inertial Measurement Unit (IMU) is necessary for precise and reliable data fusion. This procedure is crucial for applications where merging visual and inertial data improves motion estimates and spatial awareness, like flying vehicles.

Camera and inertial measurement unit calibration is done by extrinsic and intrinsic parameter calibrations and IMU coordinate system. Extrinsic calibration is determined by rotation and translation of the camera and IMU coordinate system. The intrinsic camera parameters like focal length (f_x,f_y), optical center (c_x,c_y), and coefficient distortion. Ascertain which rotation, translation, and camera matrices are used to convert coordinates from the IMU frame to the camera frame. Usually, to do this, the estimated IMU posture is used to minimize the reprojection error between the projected points and the observed pattern points in the image.

The relationship between 3D point P^{IMU} in the IMU coordinate system and point, P in the camera coordinate system is as:

$$P = K(R_{cam}^{IMU} P^{IMU} + t_{cam}^{IMU}) \tag{31}$$

Where R_{cam}^{IMU} and t_{cam}^{IMU} are rotation and translation from IMU to the camera coordinate frame, K is camera intrinsic matrix.

The camera calibration with respect to IMU is essential for accurate visual and initial data readings.

To guarantee precise and trustworthy sensor readings, calibration is a necessary procedure. You may efficiently calibrate sensors to adjust for numerous faults and enhance measurement accuracy by being aware of the different calibration forms, adhering to systematic methods, and using mathematical models. Regular calibration and validation are essential for sensors to continue functioning as intended overtime.

CHAPTER 6

SYSTEM MODEL IMPLEMENTATION

This chapter discuses and shows how the stereo camera and inertial measurement unit (IMU) fused with kalman filter in implementation of the thesis new model for an aircraft vertical landing approach in the determination of attitude, velocity and position aof an aircraft.

The system is composed of stereo camera and IMU to provide the aircraft orientation, position and velocity.

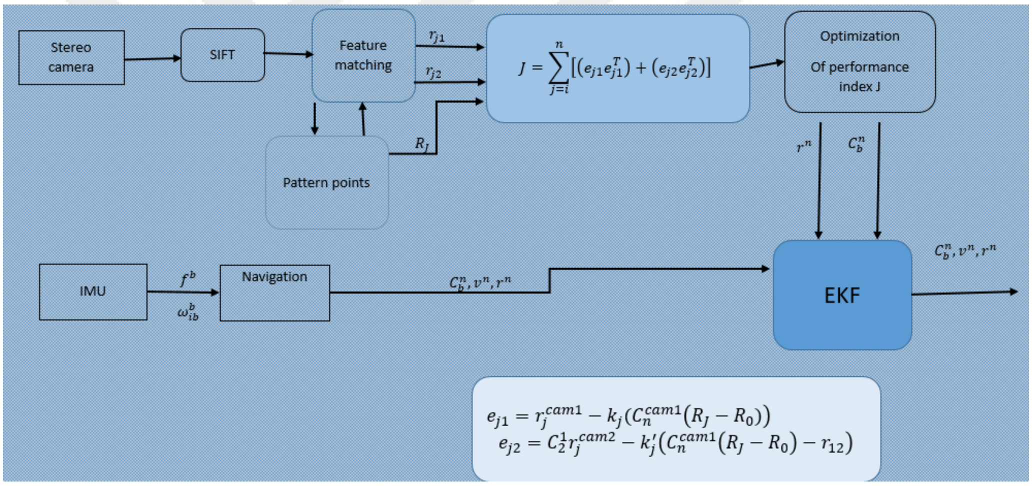

Figure 6 1**.** Stereo camera/INS fused with extended Kalman filter (EKF).

The figure 6 1 show the stereo camera/IMU system fused with extended kalman filter. Stereo camera detects features using scale-invariant feature transform (SIFT) techenique and match the detected features to the known pattern and by optimizing the stereo camera performance index equation (J) to determine position and attitude of an aircraft and an inertial measurement unit (IMU) does measure an aircraft position (Pos), orientation(Attit), and velocity (vel) by the optimizing equation (2.7-2.8) of INS. Outputs from both sensors are fused by an extended Kalman filter for linearization, estimation and get unbiased system outputs.

IMU usually use three axes to measure angular rates and determine acceleration in three dimentions (X, Y, Z).by the use of gyroscope and accerelometer data the determination of attitude, position and velocity of an aircraft is identified with relation to the reference frame.

Stereo camera may produce intricate 3D map below and surroundings of an aircraft by the use of stereo vision techniques. This is essential when flying at low altitudes where topographical precision information is critical for safe navigation.

Fusing stereo cameras with IMU for relative navigation system enhances the ability of the navigation system. By the use of the synchranized stereo cameras with high resolution the prises detection of features and depth deception are anabled. There for the position of the flying vehicles is identified. IMU being composed gyroscope and accelerometer arranged in three axises. The velocity and orientation of flying vehicle is estimated. Since the sensors outputs are not linear, the deployment of extended Kalman filter for the linearized of the sensor output estimation.

The computation of position navigation of flying vehicle in this study, using new way of stereo camera is shown below by

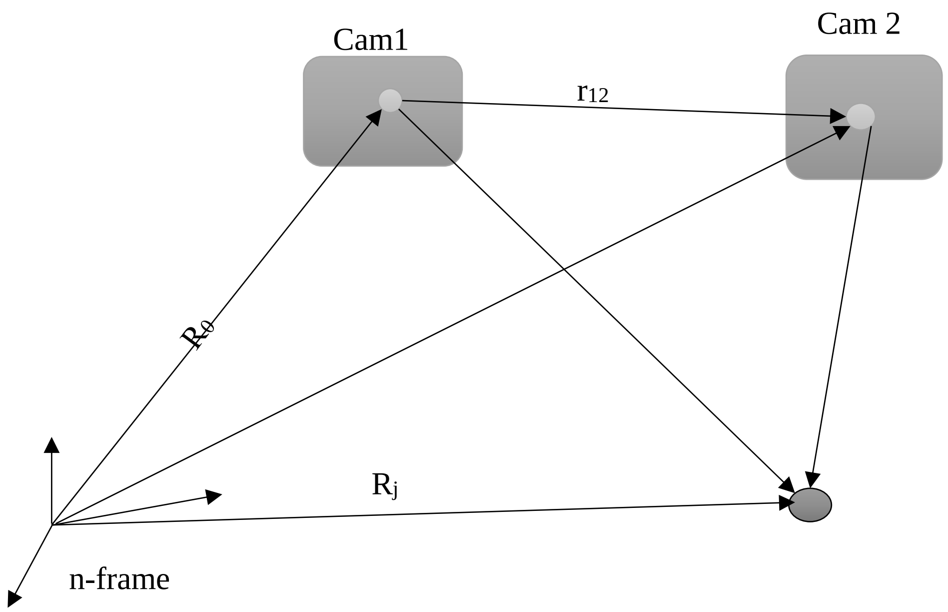

Figure 6 2**.** Navigation with stereo camera.

Using own procedure, the position vector for each camera is calculated by

$$
\begin{aligned}
r_j^{cam1} &= k_j\left(C_n^{cam1}\left(R_J - R_0\right)\right) \\
k_j' r_j^{cam2} &= C_{cam1}^{cam2} C_n^{cam1}\left(R_J - \left(R_0 + C_{cam1}^{n} r_{12}\right)\right)
\end{aligned}
\qquad (32)
$$

$$
\begin{aligned}
r_j^{cam1} &= k_j\left(C_n^{cam1}\left(R_J - R_0\right)\right) \\
C_2^1 r_j^{cam2} &= k_j'\left(C_n^{cam1}\left(R_J - R_0\right) - r_{12}\right)
\end{aligned}
\qquad (33)
$$

The equation (6.2) gives the position R_0 and orientation output C_n^{cam1} .

The performance index J is to be calculated so to optimize the system

$$
\begin{aligned}
& J = \sum_{j=1}^{n}\left(e_{j1} e_{j1}^T\right) + \left(e_{j2} e_{j2}^T\right) \\
& e_{j1} = r_j^{cam1} - k_j\left(C_n^{cam1}\left(R_J - R_0\right)\right) \\
& e_{j2} = C_2^1 r_j^{cam2} - k_j'\left(C_n^{cam1}\left(R_J - R_0\right) - r_{12}\right) \\
& \text{For } \frac{\partial j}{\partial k_{j1}} = 0, \frac{\partial j}{\partial k_{j2}} = 0, \frac{\partial j}{\partial C_n^{cam1}} = 0, \frac{\partial j}{\partial R_0} = 0
\end{aligned}
\qquad (6.3)
$$

The matrix $C_2^1 = \begin{bmatrix} cos\varepsilon & sin\varepsilon & 0 \\ -sin\varepsilon & cos\varepsilon & 0 \\ 0 & 0 & 1 \end{bmatrix}$ is known .

where ε is very small and r_{12} is a known distance between two cameras.

$$C_2^1 = (C_1^2)^T, and\ C_n^{cam2} = C_{cam1}^{cam2} C_n^{cam1}$$

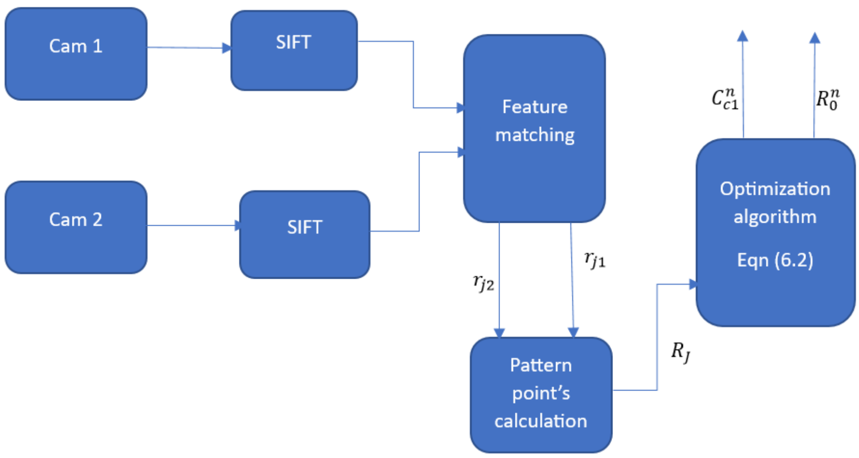

Figure 6 3. Position update with stereo navigation.

Position update from the measurement equation

$$z = Hx + v \tag{34}$$

For position update the matrix $H = [0 \quad 0 \quad I_{3\times3}]$ and system estimate $x = \begin{bmatrix} \Theta \\ V \\ Pos \end{bmatrix}$

Therefore position update $z = [0 \quad 0 \quad I_{3\times3}] \begin{bmatrix} \Theta \\ V \\ Pos \end{bmatrix}$

For altitude update $H = [I_{3\times3} \quad 0 \quad 0]$

Altitude update $z = [I_{3\times3} \quad 0 \quad 0] \begin{bmatrix} \Theta \\ V \\ Pos \end{bmatrix}$

Fusing the updated and calibrated stereo camera with an IMU provides real-time robustness and accurate system output. An IMU is composed of three-axis gyroscopes and accelerometers.

Stereo cameras fusing with data from an inertial measurement unit (IMU) using an extended Kalman filter improve the position and orientation accuracy estimation over time [10], [31].

CHAPTER 7

TEST AND RESULTS

In this part the flying vehicle modeling has been simulated in MATLAB to evaluate the effectiveness and behavior output reliability of the algorithm of using stereo camera / IMU for the relative navigation system using an extended Kalman filter for estimate linearization. The applied flying vehicle simulation period is 60 seconds since the altitude is low up to 200m as the simulation altitude. The roll and pitch angles are conditioned not to exceed 15 degrees and the landing approach has to be verticle landing. The comparison of nominal and algorithm simulation results is shown in the figures below.

It is composed of five sections. The first section includes the simulated results using INS/GPS (nominal) to test the orientation, velocity, and position propagation of a flying vehicle at low altitude and approaching to land at the known pattern. The second part provides the variations of the flying vehicle's orientation, velocities, and position by using the INS/Stereo camera approaching to land at the known location. The third section is the comparison of the first two sections for the relative navigation system. The forth section is composed of the error analysis and comparison of results when using pure INS, stereo cameras/IMU and GPS/IMU. And the fifth section which is the last part of this chapter is the study the stereo cameras/IMU and GPS/IMU standard deviation propagation.

7.1 Nominal simulation results

The nominal simulation is the errorless simulation results for relative navigation systems is identified when INS/GPS has excellent satilitte signals and this serves as a good choice in navigation systems in various applications including aviation navigation systems. Using the Matlab environment the simulation using this navigation system, the variations of flying vehicles were tested and the results were studied, and found that it has low inaccuracy and this makes it reliable regardless of the other factors that could affect its accuracy.

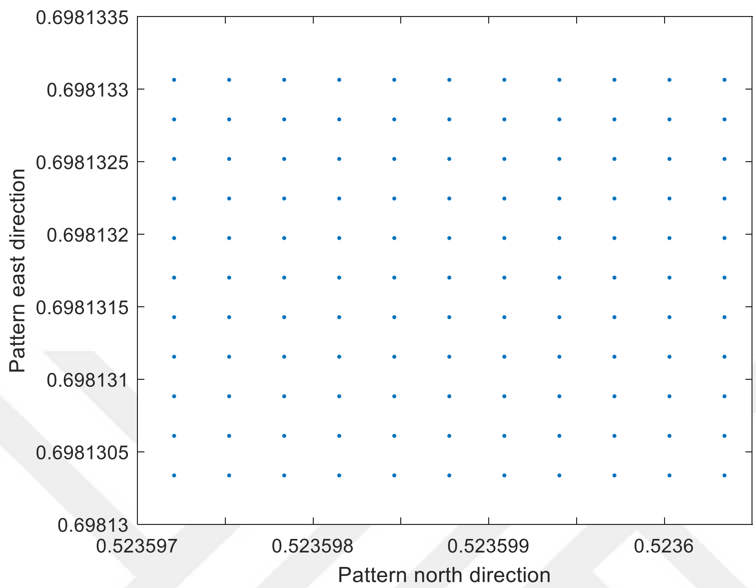

Figure 7 1: Pattern points

Figure 7.1 shows the pattern points of which an aircraft visual navigation detects and land on it vertically.

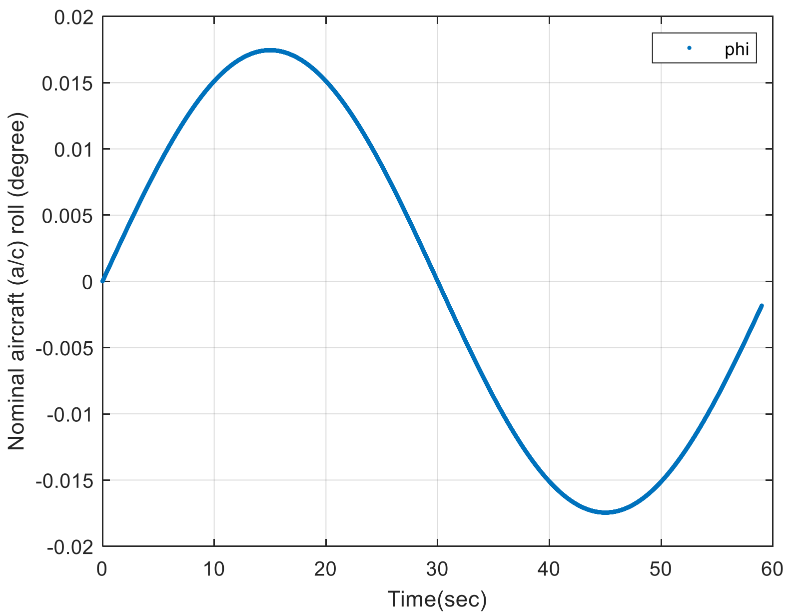

Figure 7 2: Nominal roll of an aircraft

Figure 7.2, is a simulation nominal roll of an aircraft in 60 seconds. It shows uniform and stable sinusoidal formation.

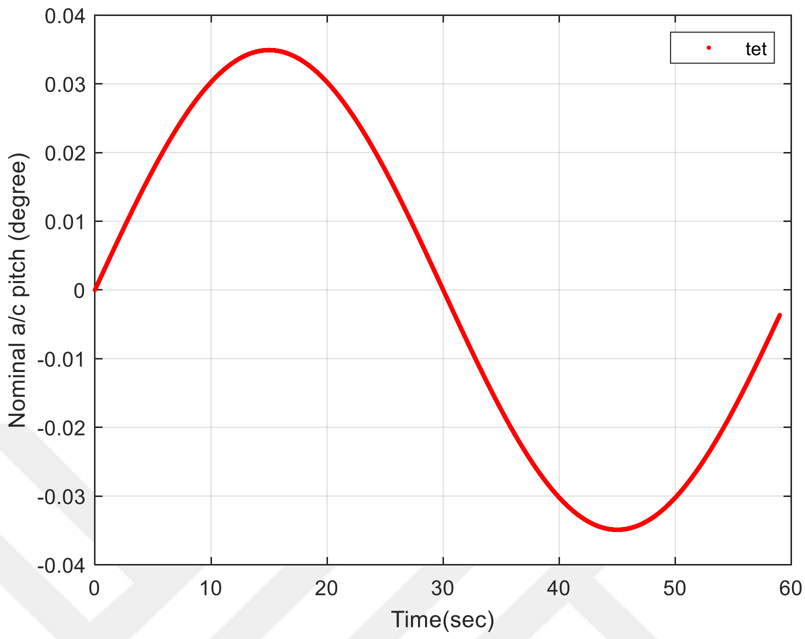

Figure 7 3. Nominal pitch of flying vehicle.

Figure 7.3 shows the sinusoidal aircraft errorless (nominal) pich formation. The simulation results on pitch behavior shows stable propagation.

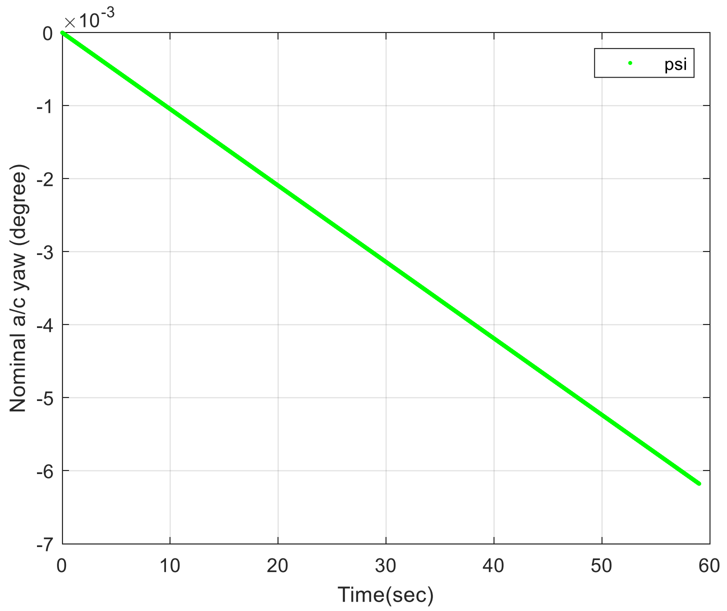

Figure 7 4. Nominal yaw

Nominal yaw behavior of an aircfraft shown on figure 7.4 justfies that it decreases as time increases when the aircraft keeps on approaching to land. The nagative sign shows the direction of yaw (left yaw).

The propagation of roll, pitch, and yaw nominal navigation shows the real-time propagation of flying vehicles during their maneuvering performance with in 60 seconds time bound.

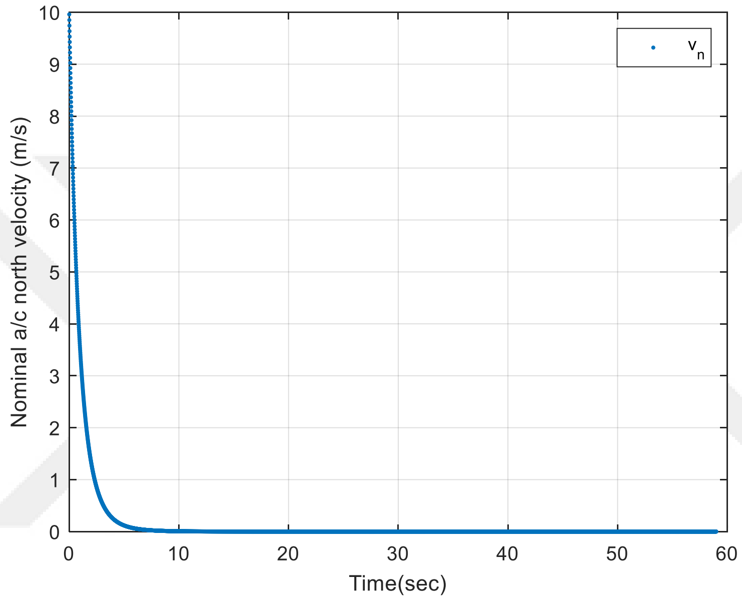

Figure 7 5. Nominal north velocity

The figure 7.5 shows the variation of north (x- direction) velocity in 60 seconds. Simulation shows that north velocity initial velocity is high which quickly reduced with in 6seconds and becomes stable at zero the rest of the simulation time.

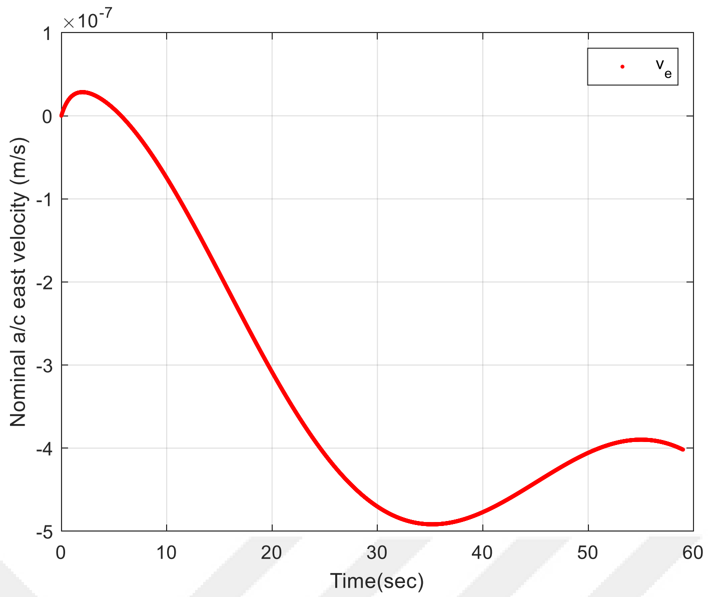

Figure 7 6. Nominal east velocity

Figure 7.7 shows the variation of east (y-diraction) velocity. Initially it increased for some few seconds (3 seconds) and gradually decreases uniformaly up to about 30 seconds and non-uniformly variates the rest of the simulation time. This has no effect on accuracy since the whole simulation results are very very small (near to zero).

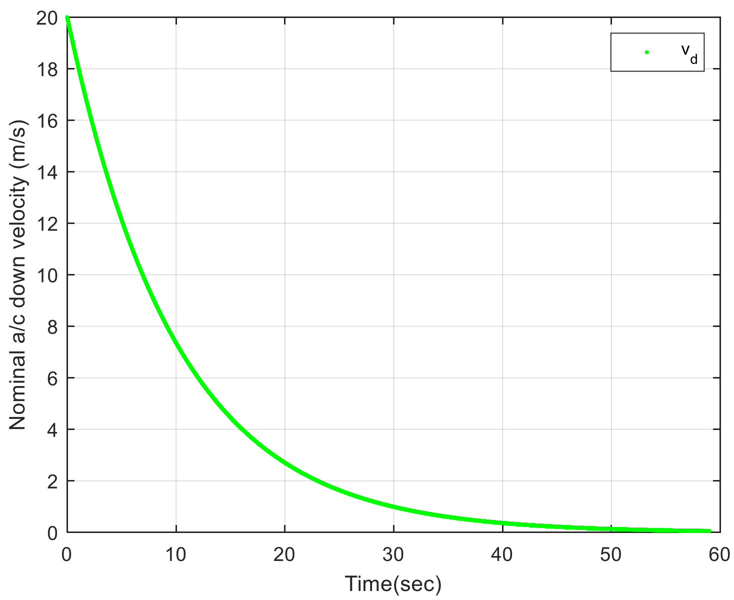

Figure 7 7. Nominal down (z-direction) velocity

This figure 7.8 shows the smooth gradual down velocity variation of an aircraft. Down velocity simulation shows that it decreases as the aircraft approaches landing time till it reaches to zero velocity. This makes it useable and reliable for flying vehicles in navigation systems.

Looking at the propagation behavior of velocities in all three (north, east, and down) directions indicate that the nominal velocities in navigation systems on which the reference is taken.

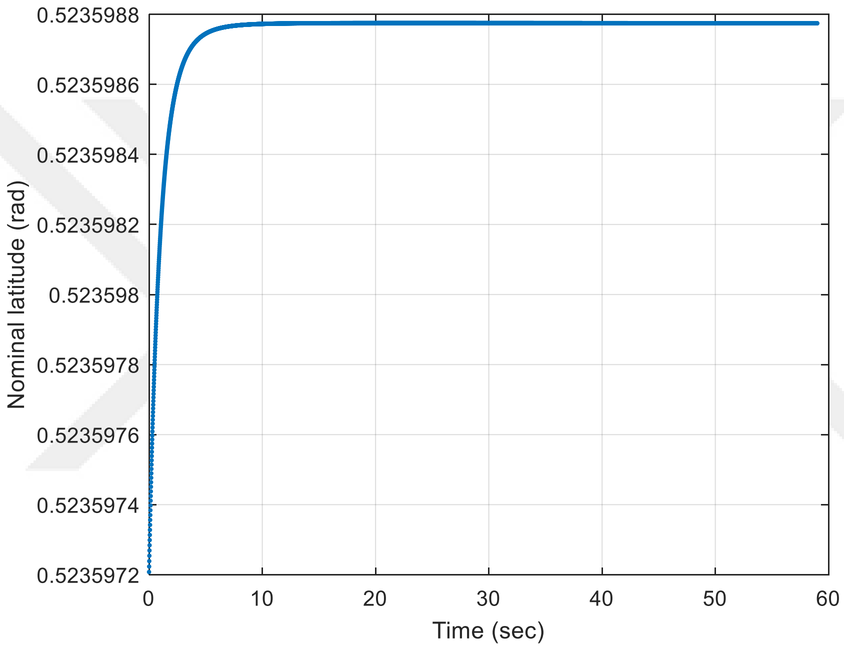

Figure 7 8**.** Nominal latitude

Given the range period of time shown in figure7.10, by nominal navigation the latitude behavior of flying vehicle with respect to time is studied. The simulation shows the uniform horizontal variation as the time of flight goes to zero. Up to 10th second the latitude starts to decrease to zero.

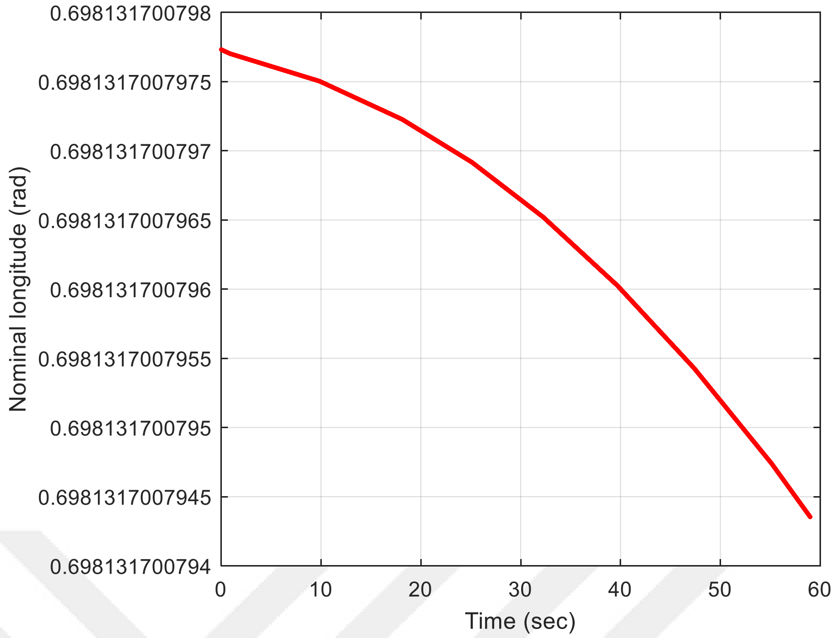

Figure 7 9. Longitude nominal navigation against time

Figure 7.11 shows that the nominal longitude keeps decreasing as the aircfrat aproaches to land. At the inital start, the longitude is high and goes down as the landing time approaches.

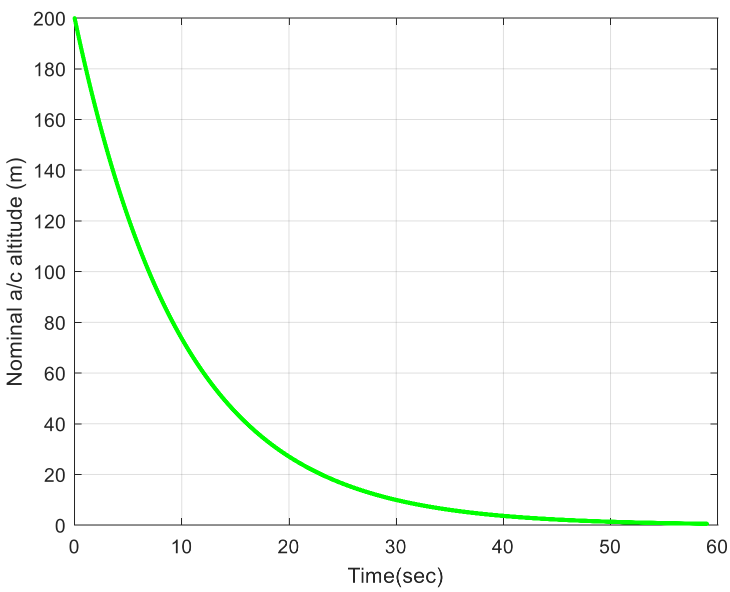

Figure 7 10. Nominal altitude

Simulation shows the gradual decreas of nominal altitude as the aircraft goes down to land. Figure 7.12 shows the nominal altitude from 200meters to zero with in about 60 seconds.

Based the propagation of simulated graphs showing changes of the flying vehicle in its nominal position variation with time, it is seen that the nominal navigation for relative navigation system gives accurate and reference readings

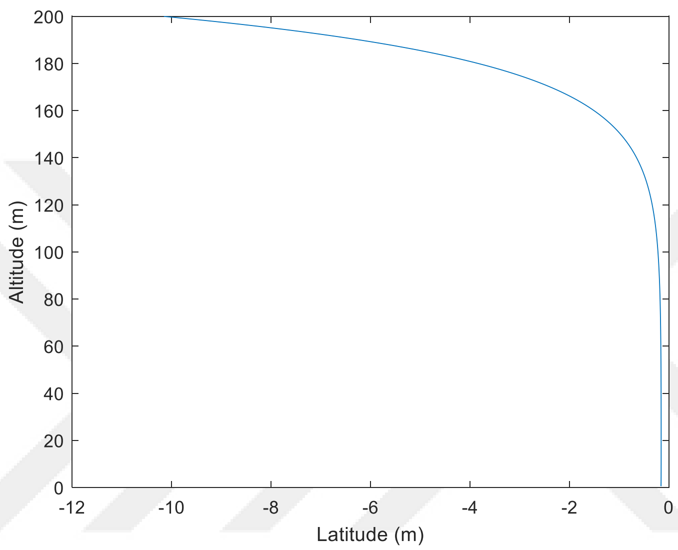

Figure 7 11**.** Nominal vertical flight path.

Figure 7.14 shows the nominal flight trajectory of an aircraft from 200m altitude to the ground. The graph shows that the latitude is inversely propotipnal to altitude. Latitude increases as the aircraft altitude decreases as it goes to the pattern.

7.2 Test and Results Using Camera

This section the flying vehicles attitude, velocities and position are tested using by integrating stereo camera for relative navigation system to check the variation behaviors accuracy of this vehicle approaching to the know pattern. The use of stereo cameras for relative navigation is expected to be more reliable in navigation systems since it only requires no external signal sources. Below are the simulated results showing the attitude, velocity, position, and flight trajectory of the flying vehicle using the stereo camera.

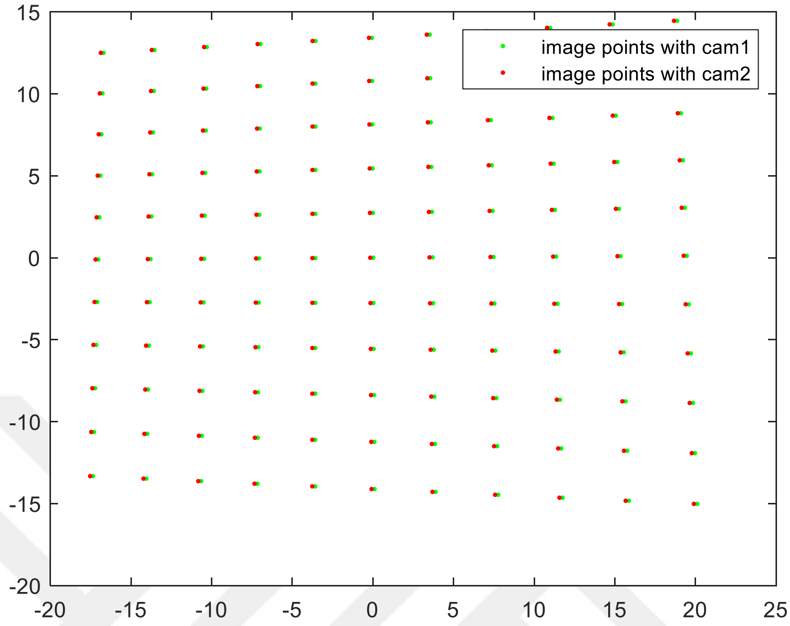

Figure 7 12. Stereo camera/IMU points

The figure 7.15 shows the points of two calibrated cameras' focus relative to one another. This provides the accuracy of image points by comparing the image point in camera one with respect to camera two. Both cameras view points from different view poses but at any point, each camera point is almost matched to one another camera. Hence both cameras have the same focus and this shows that the stereo camera is well calibrated.

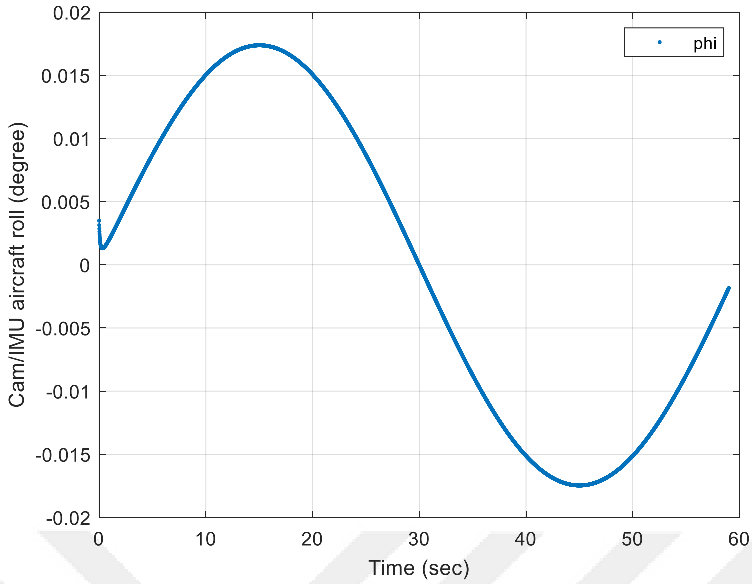

Figure 7 13**.** Stereo camera/IMU roll

Figure 7.16 shows the aircraft roll variation angles in 60 seconds where the simulation shows that the roll obeys uniform sinusoidal variation. At about 60th second roll angle is zero. The siimulation shows that aircraft rolls right- left manouver.

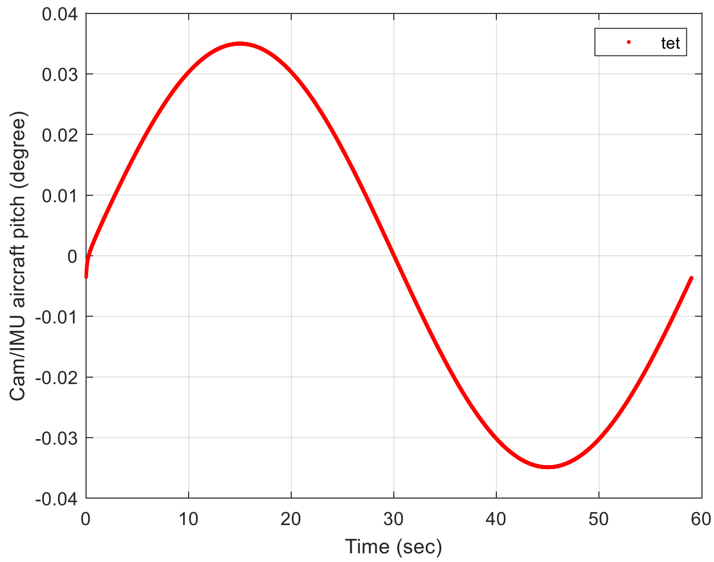

Figure 7 14. Stereo camera/IMU aircraft pitch

Figure 7.17 shows the aircraft pitch variations. The sinusoidal form indicates that aircraft can maneuver both up and down.

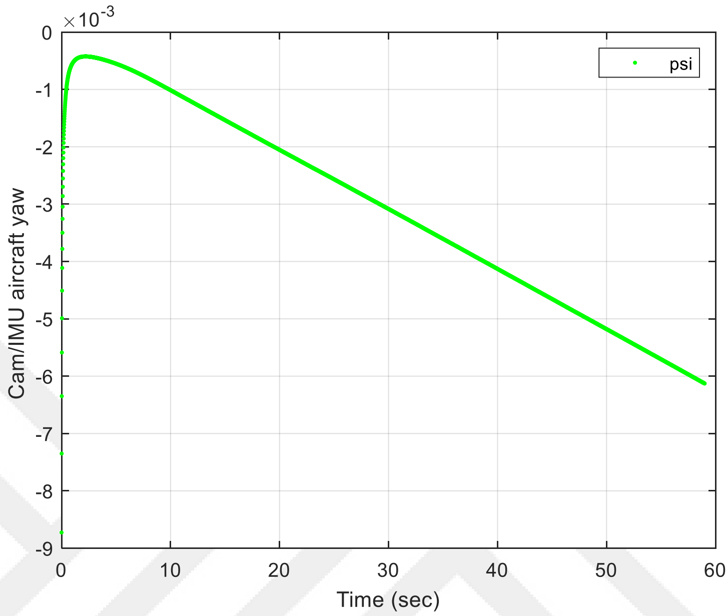

Figure 7 15**.** Camera/IMU aircraft yaw variation

Figure 7.18 shows that the aircraft yaw using stereo camera/IMU navigation. Initially, the yaw angle was high in the left (left-right) direction which quickly reduced nearly to zero angle and linearly increased with time up to 0.005 degrees in almost 60seconds.

The use of a stereo camera shows that it is a better choice for the relative navigation system in the determination of an aircraft attitude since this system's signal dependency does not require any external signal source. This makes it reliable based on the accurate attitude behaviors of flying maneuvers.

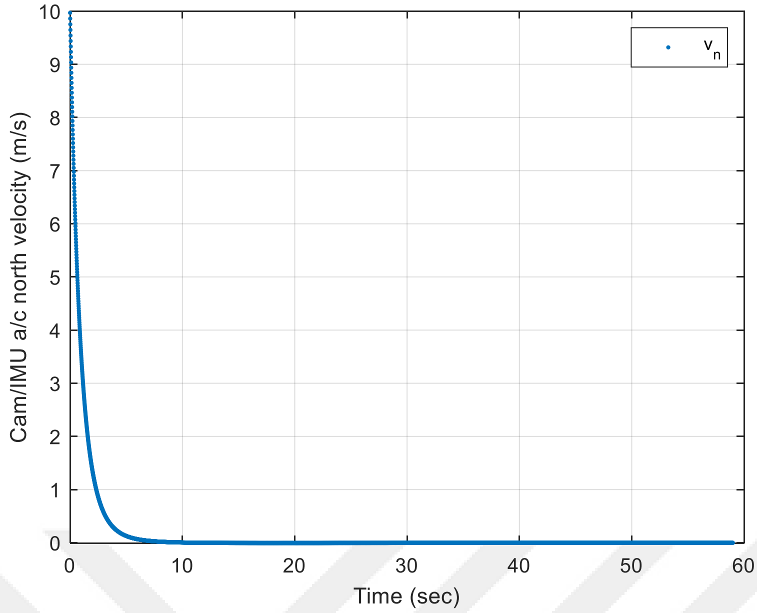

Figure 7 16. North velocity (x-direction velocity) using the camera/IMU

Figure 7.20 shows how the simulation results of north velocity decreases rapidly to zero within about 6 seconds and constitantly variate to zero with in the remaining time bound for the aircraft performs a vertical landing the variation of north velocity approaches to zero.

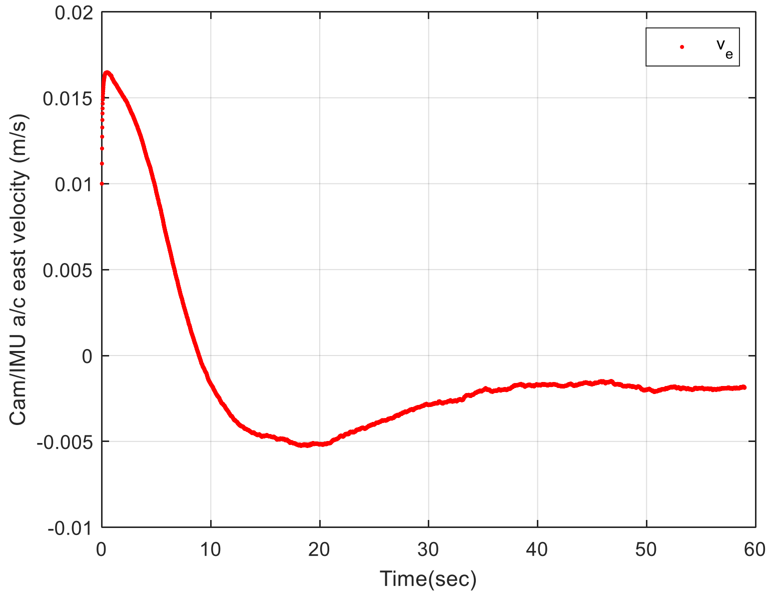

Figure 7 17. East velocity using camera/IMU

Figure 7.21 shows the behavior of an aircraft's east (y-direction) velocity against flying time approaching its vertical landing. Initially, east velocity increased up to 0.016 m/s and gradually decreases to nearly zero. The simulation result shows that for vertical landing the variation of east velocity is small and keeps decreasing to zero.

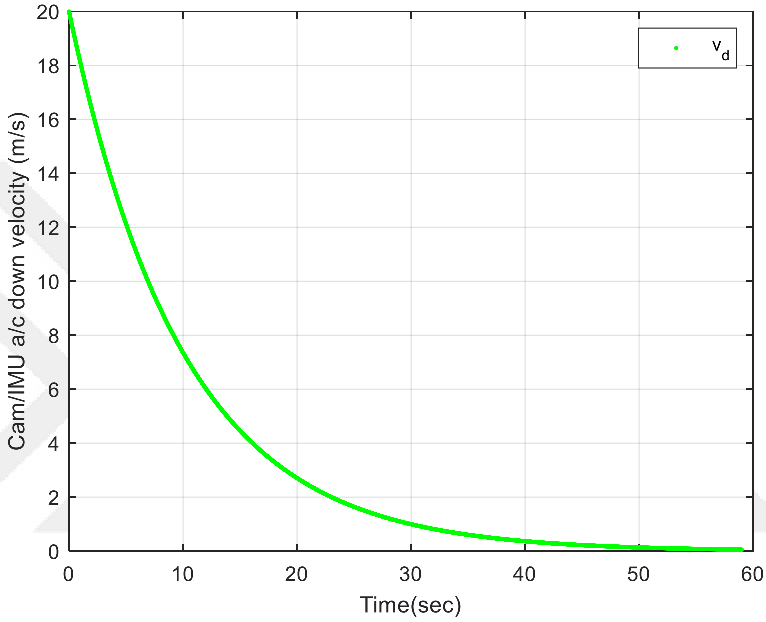

Figure 7 18**.** Stereo camera/IMU down velocity

Figure 7.22 shows the simulated down (z-direction) velocity behavior when an aircraft approaches to have its verticle landing on a pattern. Down velocity shows parabolic decreas pattern as the aircraft approches the pattern vertically landing.

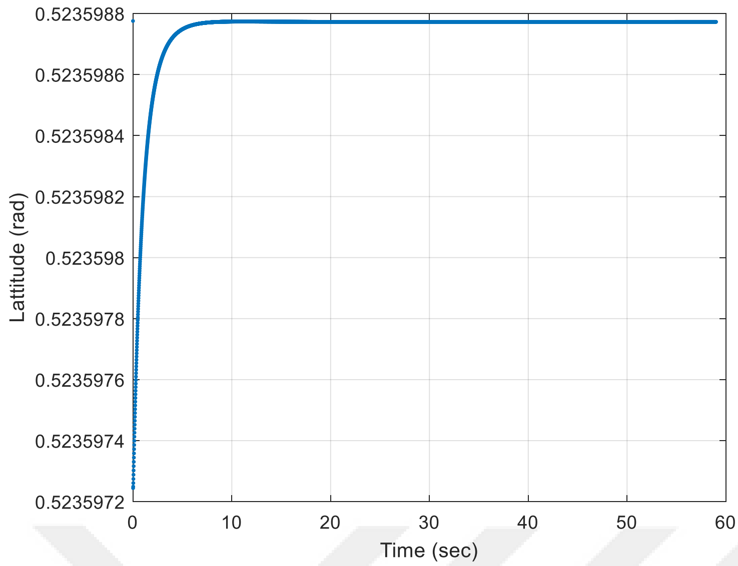

Figure 7 19. Stereo cam/IMU latitude variation

Figure 7.24 shows the behavior of aircraft navigated latitude position when coming to the pattern vertically landing. The simulation graph shows the latitude is stable and uniform when an aircraft is at its cruising altitude and starts to decrease as the aircraft descends vertically toward the landing pattern.

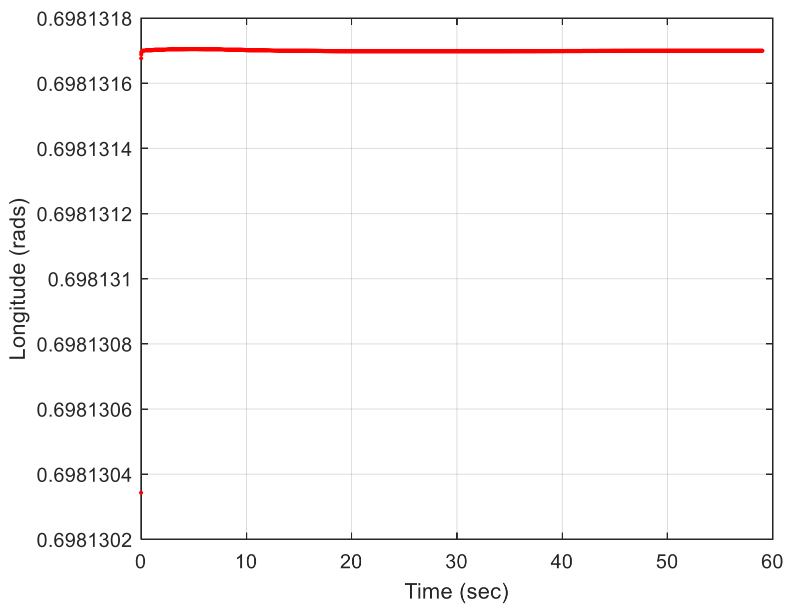

Figure 7 20. Stereo camera/IMU longitude variation.

The figure 7.25 shows that the simulation parameter (longitude) initially quickly increased and kept uniform throughout the landing time.

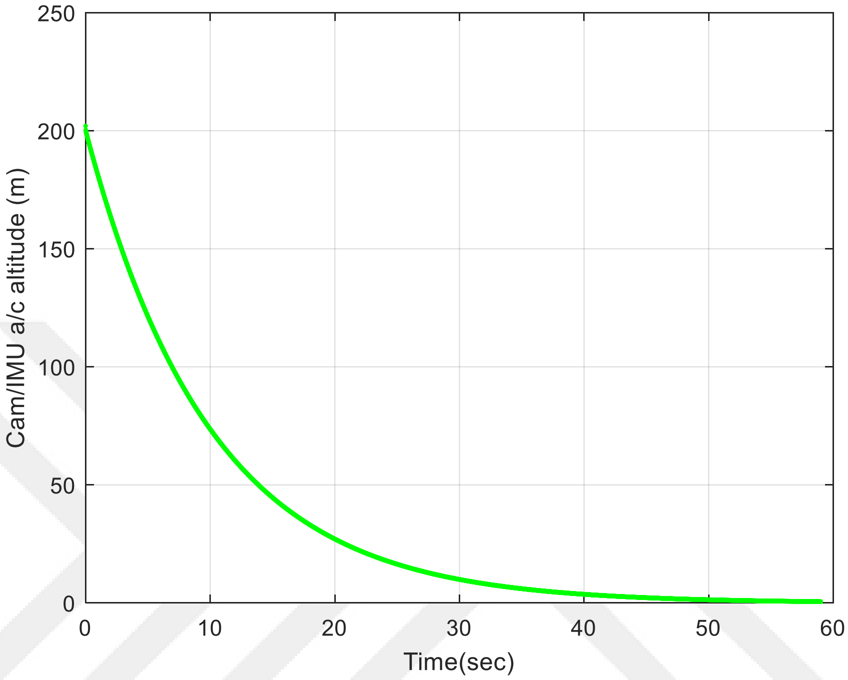

Figure 7 21**.** Stereo camera/IMU altitude variation

The figure 7.26 shows the parabolic altitude decrease when navigating using stereo camera/IMU fused with extended kalman filter. The altitude is vertically decreased as the aircraft verticaly approaches the landing pattern.

Based on the simulation results of aircraft position variation as it comes to land, shows the smooth and accurate variation towards the known location over time. This justifies that the use of cameras for relative navigation systems is a solution for vehicle position identification.

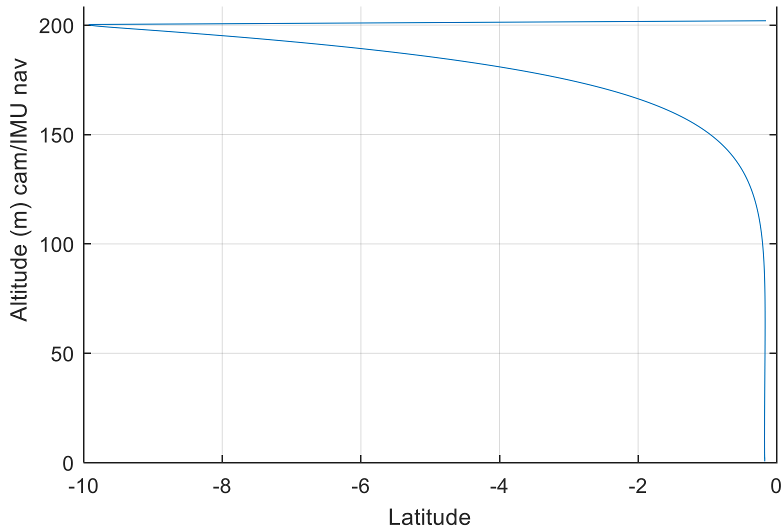

Figure 7 22**.** Stereo camera/IMU flight path

The figure 7.27 shows how to use camera/IMU tracks the flight path of a flying vehicle. The trajectory path shows the cruising altitude of an aircraft and when it reaches 200 m the aircraft starts to descend and landed vertically on a pattern.

7.3 Comparison Between nominal and Stereo Camera/IMU Navigation

The below-simulated results provide the comparison between nominal navigation and stereo cameras/IMU for the relative navigation system. The results were studied and compared to come up with the new idea of using stereo cameras for relative navigation systems of flying vehicles mostly at low altitudes since cameras do not require external signals and GPS does require signals from the number of satellites.

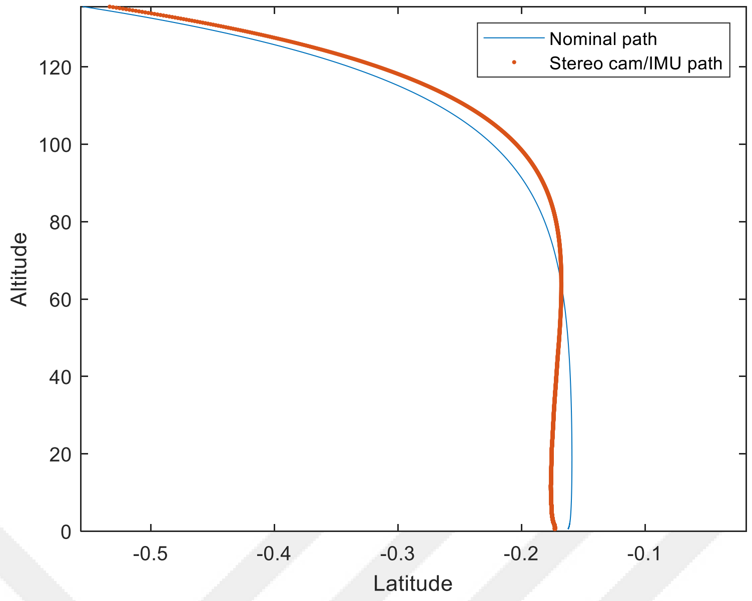

Figure 7 23**.** Nominal and Camera/IMU aircraft trajectory

The figure 7.28 shows the comparison aircraft trajectory between nominal and stereo camera/IMU. The simulation shows that navigation using camera/IMU is almost accurate as nominal. This proves that the cam/IMU could alternatively be used in flying vehicles' navigation.

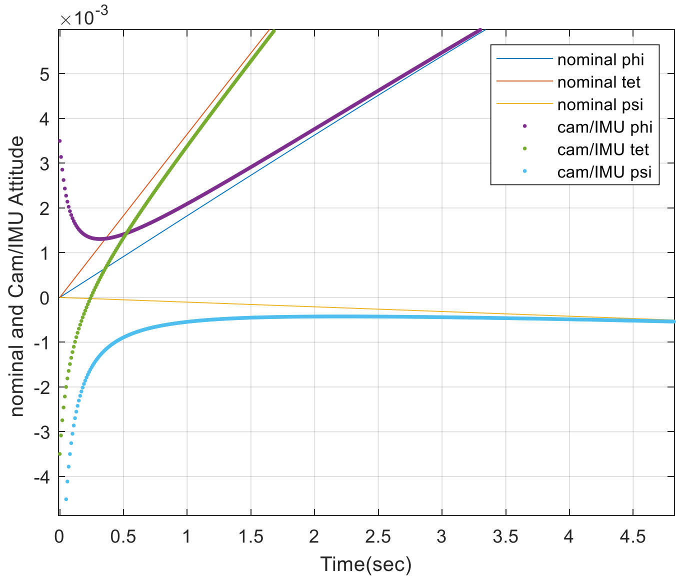

Figure 7 24**.** Nominal and stereo camera/IMU orientation navigation comparison

The figure 7.29 shows the zoomed behavior nominal and stereo camera/IMU airacraft attitude navigation. It shows that there is a very small difference between errorless navigation and camera/IMU during the initial navigation which converges to become in-line with nominal orientation variations.

Based on the simulated graph above indicates almost no differences in roll, pitch, and yaw propagation over time and maneuver when navigating using camera/IMU compared to errorless navigation state. This makes a stereo camera/IMU to be an alternative and a better choice in a navigation environment.

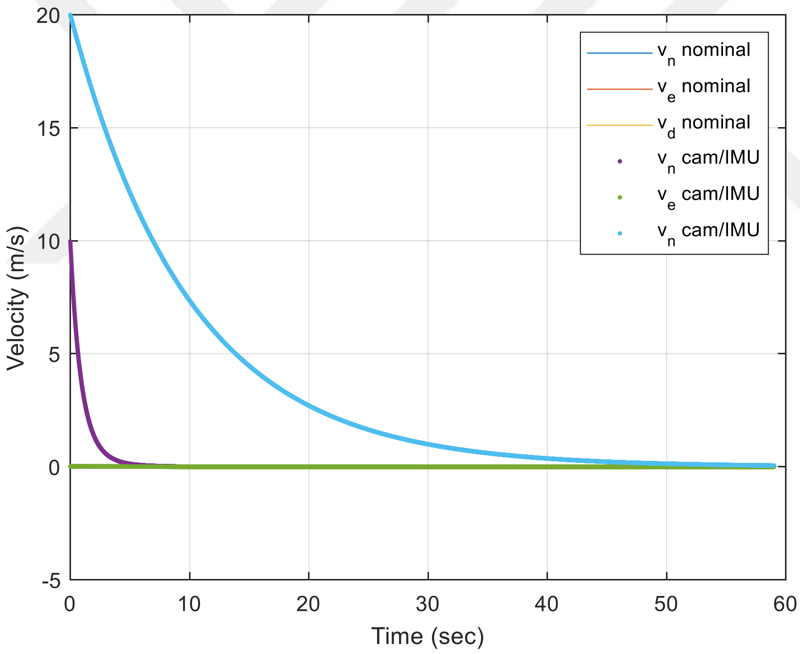

Figure 7 25**.** comparison of nominal and stereo camera/IMU velocity.

Figure 7.30 shows that for all nominal and stereo camera/IMU velocities (north, east, and down velocities) the propagation over time shows the same results. This means that by using the stereo camera/IMU for the relative navigation system, it is possible to get the same results hence the alternative solution in the navigation world.

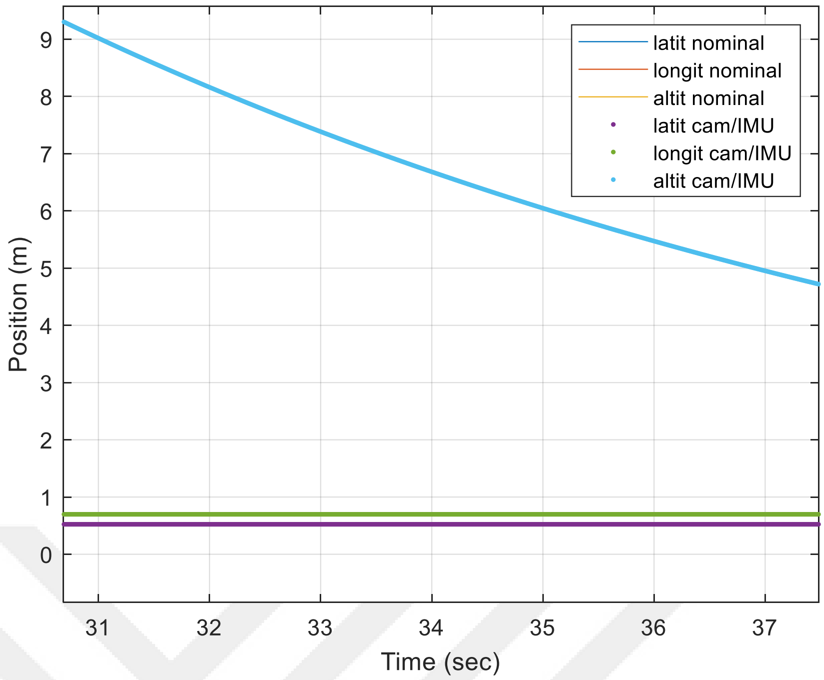

Figure 7 26. Nominal and stereo/ IMU position comparison

The simulation traces the behavior of a flying vehicle comparing camera/IMU position behavior as shown in figure 7.31 and the simulation shows the similarities variation for all aircraft position parameters (latitude, longitude, and altitude). Position with camera/IMU navigation being in line with that of nominal navigation for relative navigation shows that the integration of a stereo camera and IMU for relative navigation can work smoothly to provide reliable output at a low cost and altitudes since it does not require external signal sources.

7.4 Error Propagation When Navigating With Pure INS and Stereo Cameras/IMU and GPS/IMU

This section shows the error simulated behavior when using pure INS, stereo camera/IMU, and global positioning system (GPS)/IMU inertial measurement unit. These simulated error results helps in system error analysis in comparison to one another and hence coming up with the reliable system

7.4.1 Pure INS Error

The study of error propagation when using pure INS in comparison with stereo camera/INS provides the chance to choose which system is to be considered most and the feasibility of the system. The below graphs show the error behaviors using INS.

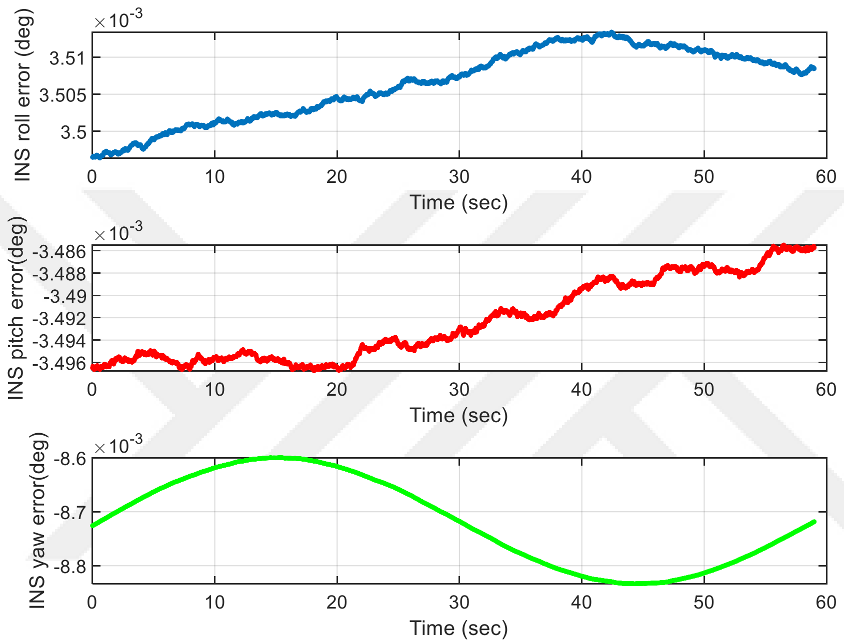

Figure 7 27**.** aircraft orientation errors.

This figure 7.32 shows that when navigating with pure INS, the aircraft experiences unstable roll and pitch error propagation. The maximum errors are 0.0035 deg roll, 0.0034deg pitch and 0.0086 deg yaw. This means that navigating with pure INS orientation errors and control is expensive. Depending on the pure INS navigation parameters is not good ideal since it exposed to unstable error varriations.

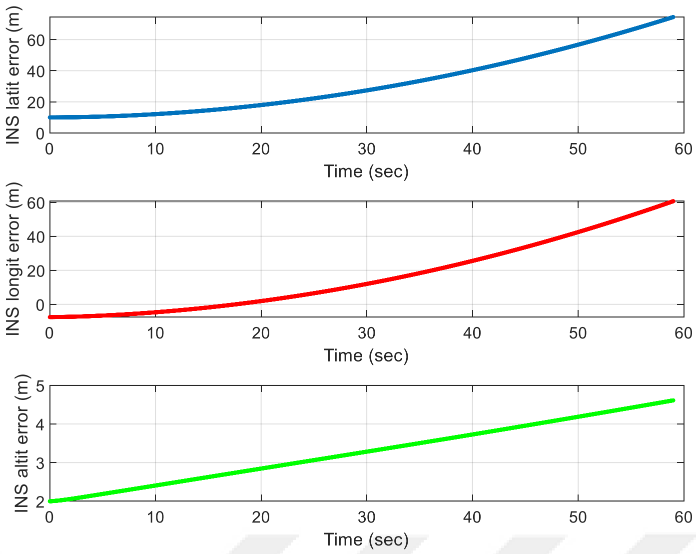

Figure 7 28**:** Position error using pure INS

The figure 7.33 shows that the position error with pure INS navigation gradually increases over time. Using pure INS, the aircraft experiences very high altitude, longitude, and lattitude error variation. Pure INS is not system to be used for flying vehicle position identification.

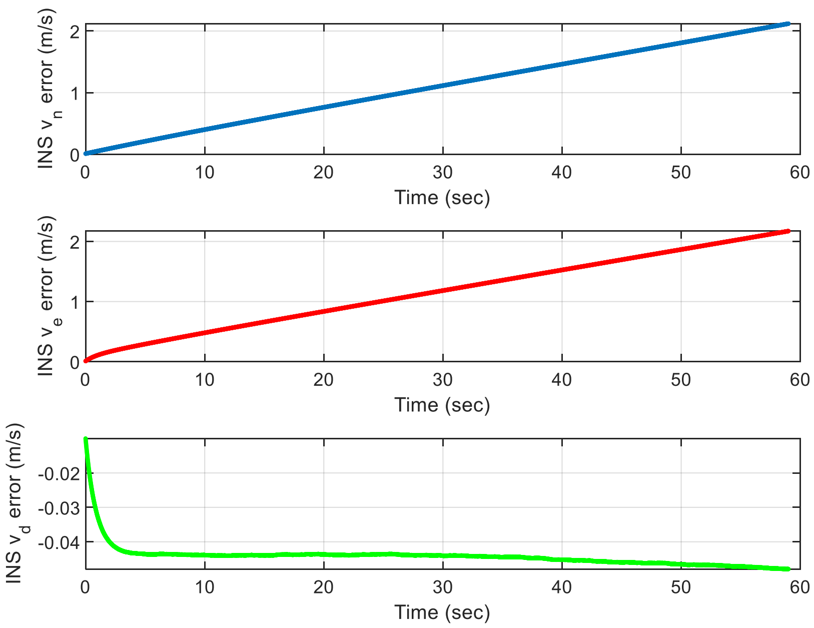

Figure 7 29**:** Pure INS velocity error

Figure 7.34 shows the unstable variation errors of aircraft velocities when navigating using a pure inertial navigation system. The gradual increase in variation error in aircraft north, east velocity, and unstable down velocity shows pure INS navigation is prone to high-velocity errors hence INS can not sustain navigation for flying vehicle alone.

7.4.2 INS/Stereo Camera Errors

This part shows the simulated error results when using the stereo camera for relative navigation system and compare them to that of pure INS so that the feasibility of the new system model. The more stable error output over time the easier and cheaper the calibration cost.

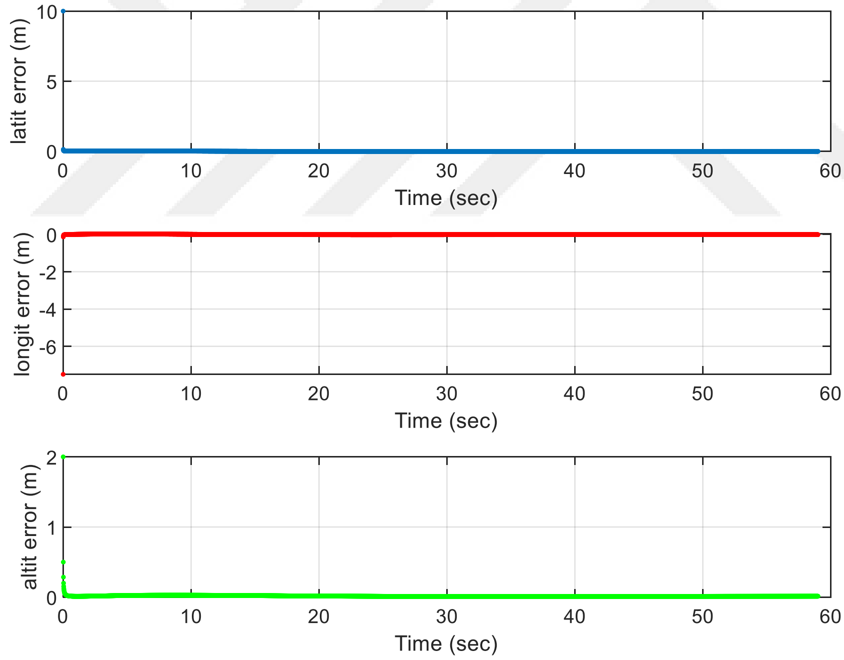

Figure 7 30**:** Position error behavior with stereo Cameras/INS

Figure 7.36 shows that the error variation when an aircraft navigating with stereo camera/IMU the position error is diminished and stable. This means that the position navigation output is reliable and cheap to mitigate resulting errors. 0.02m altitude, 0.004m longitude, and 0.0014m latitude aircraft simulation errors were identified when navigating with stereo camera/INS

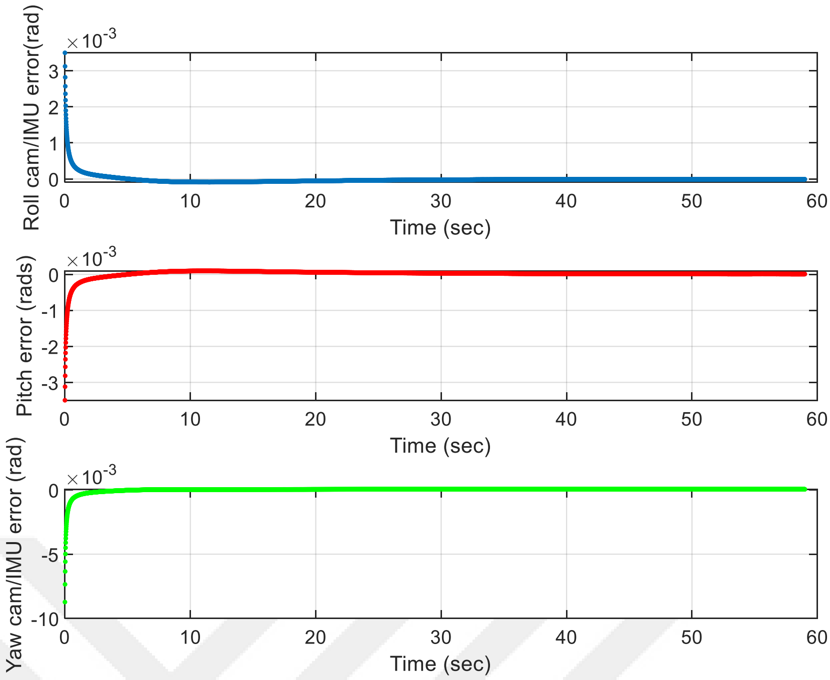

Figure 7 31**:** Orientation error behavior with stereo cameras/ INS (IMU)

The figure 7.36 shows aircraft orientation errors when navigating with stereo camera/IMU and shows $2.5 \times 10^{-4} rads$, $7.6 \times 10^{-5} rads$, and $6.3 \times 10^{-6} rads$ maximum error roll, pitch, and yaw respectively. The overall orientation errors are very very small and makes this new system accurate and reliable.

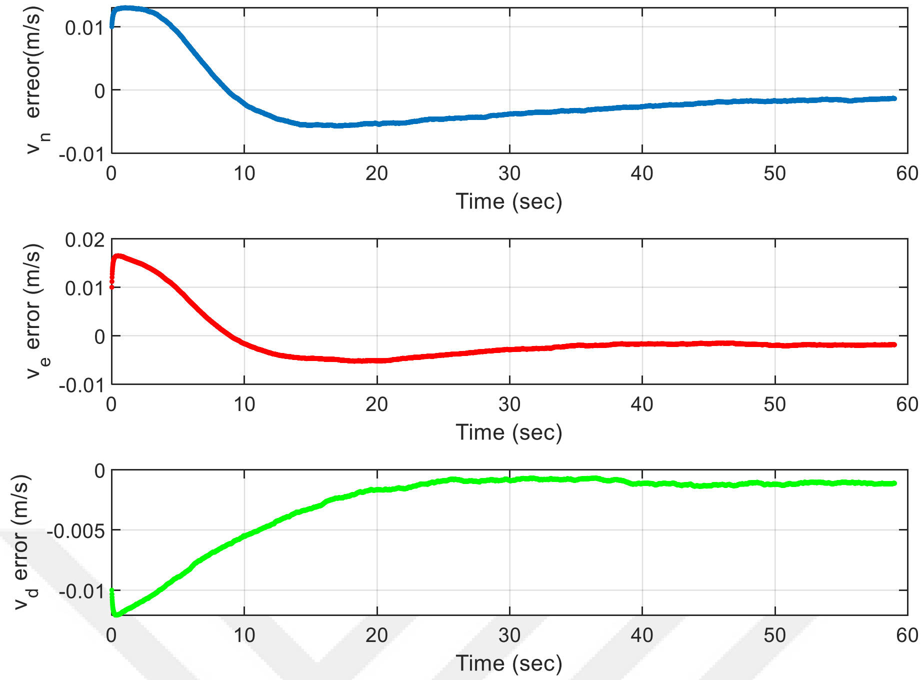

Figure 7 32**:** Velocity error behavior with stereo camera/INS (IMU)

The simulation figure 7.37 shows that the velocity maximum error with stereo camera/INS is stable and converges to zero within few seconds from its initial none zerom errors. The maximum north, east, and down velocity errors simulated shows $1.3 \times 10^{-2} m/s$, $1.6 \times 10^{-2} m/s$, and $3 \times 10^{-4} m/s$ respectively. These errors are very small and has no effect on the system accuracy and control.

Overall simulated error analyisis shows that pure INS provides unstable errors for all orientation, velocity and position parameters of flying vehicles. The integration of stereo camera/INS results to stable and deminished errors over time. Therefore the use of stereo cameras and IMU for relative navigation of flying vehicles is a very nice choice since the system require no external signal sources with less and stable errors.

7.4.3 GPS/IMU Navigation Errors Propagation

This section shows the orientation, velocity, and position error propagation when navigating with GPS/INS. It was seen that GPS/INS integration is an excellent choice when the GPS recieves an interrupted signals from at least 4. The below figures shows error propagation in navigation while experiencing the real world including factors that affects GPS signals.

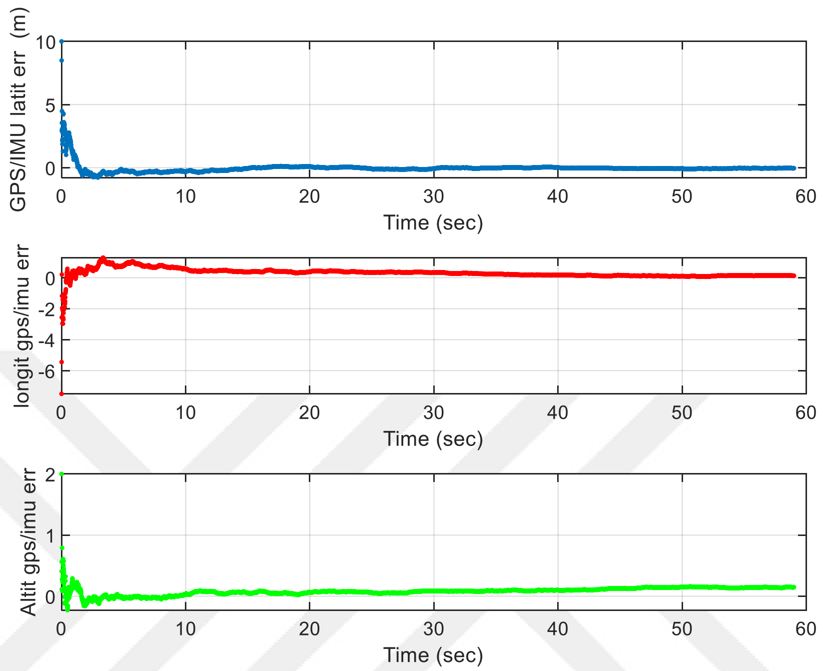

Figure 7 33**:** Position error variation with GPS/IMU

The figure 7.38 simulation results show that aircraft positioning when navigating with GPS/INS in real performance mostly at low altitudes is prone to small unstable errors. 0.01m, 0.0097m, and 0.028m are the latitude, longitude, and altitude simulated maximum errors respectively. Depending on the unstablity of error variation due to the signal distortion from sattelites, the mitigation control is almost imposible since the navigator has no action on sattelite relocation hence expensive to mitigate the errors of GPS at low and signal distructive envirnoment.

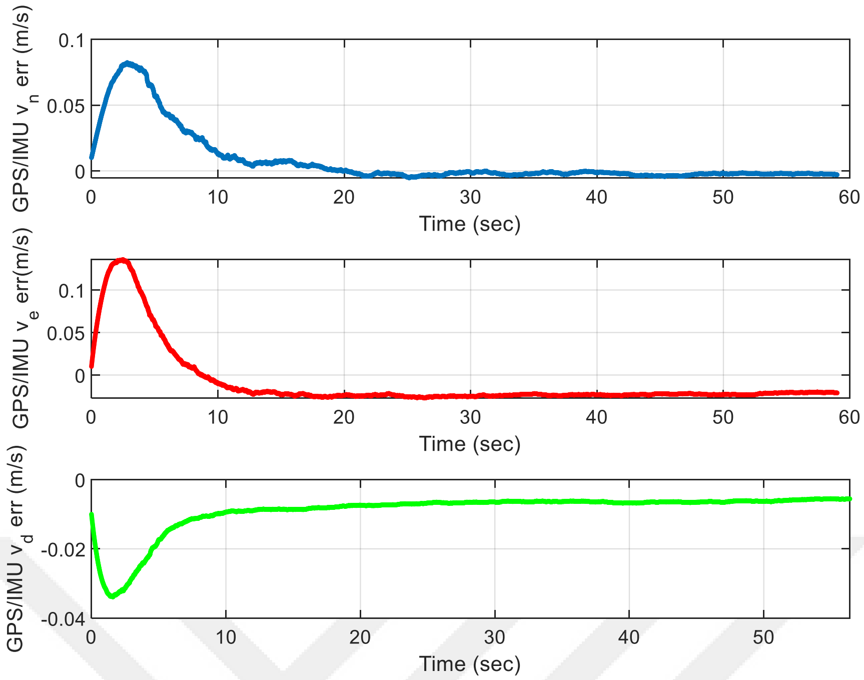

Figure 7 34**:** Velocity errors propagation with GPS/IMU

The simulated velocity propagation in figure 7.39 shows that the maximum error variation occurs at its initial time (10 seconds) but converges approximately to nearly zero. The variation error shows less stable error variation for all north, east, and down velocity variations. The maximum errors down , east, and north velocity identified are 0.0068m/s at 41second, 0.135m/s at 2second, and 0.08m/s at 3second respectively. Having been unstable errors when navigating with INS/GPS, makes it difficult to mitigate the resulted errors and this may lead the system to be unreliable mostly in an environment with less satellite signals to GPS.

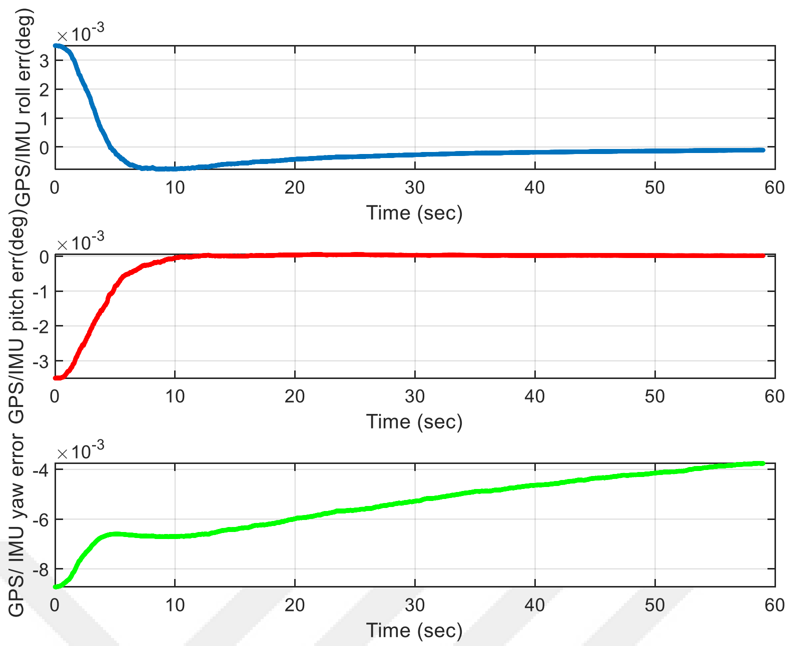

Figure 7 35: Orientation errors

The simulation results in fig 7.40, shows the less stable orientation errors are experienced in real GPS/IMU for relative navigation system. The less stable and converging roll,pich, and yaw degrees are resulted when simulating real GPS/IMU navigation.

Table 1: Table showing system amaximum errors

System	Max roll error (radians)	Max pitch error (radians)	Max yaw error (radians)	Max north velocity error (m/s)	Max east velocity error (m/s)	Max down velocity error (m/s)	Max latitude error (m)	Max longitude error (m)	Max altitude error (m)
Pure INS	0.003	0.0035	0.0086	2.12	2.17	0.044	74	60	4.5
GPS/INS	0.003	5.45e-05	0.0038	0.853	0.136	0.034	0.69	0.86	0.308
Cam/INS	0.00025	7.6e-05	6.3e-06	0.853	0.016	0.0003	0.01	0.0097	0.028

7.5 Standard Deviation

This section shows the simulated results when navigating with stereo camera/IMU and the deviation when navigating with GPS/IMU. The standard deviation shows the capability of the system in which it can consistently maintain the standard measurement or deviate from the nominal standards.

7.5.1 Stereo Cameras/IMU Navigation Standard Deviation Behavior

System standard deviation simulation is done to determine the similarity and the dissimilarity level of the system output and to enhance the linear contrast in image processing. The blow graphs show the simulated standard deviation behaviors of various parameters of flying over time.

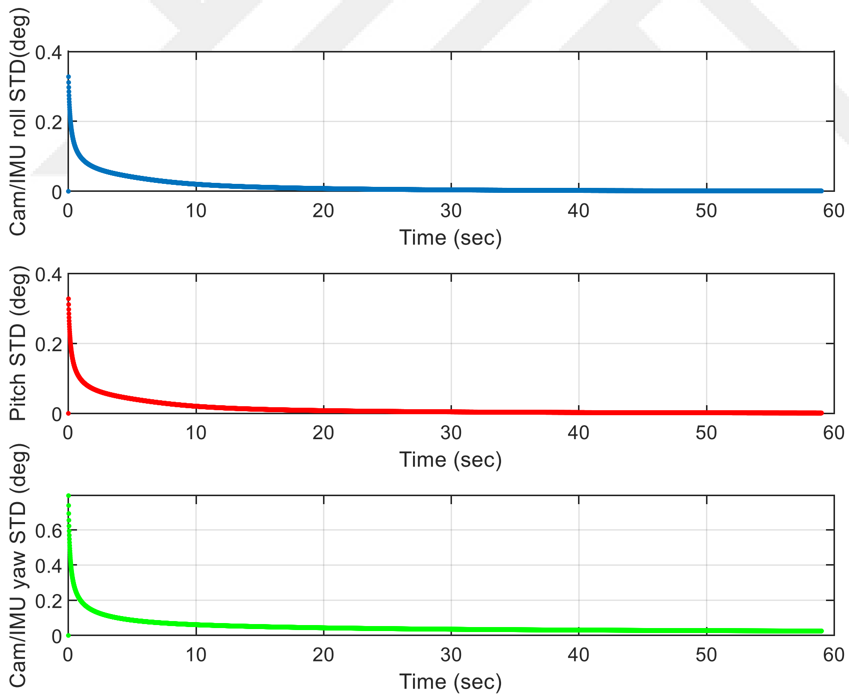

Figure 7 36**:** Orientation standard deviation

In the figure 7.41, the simulation shows that the orientation system deviation is very small and converges rapidly near to zero over time. The deviation is very less when navigating with camera/INS and this justifies this new system being reliable and standardized system for aircraft orientation relative to known pattern at low altitude.

Considering the simulation results, shows that the deviation with cam/IMU gradually converge with in short period of time. This makes the system orientation accuracy reliable and real time robustness.

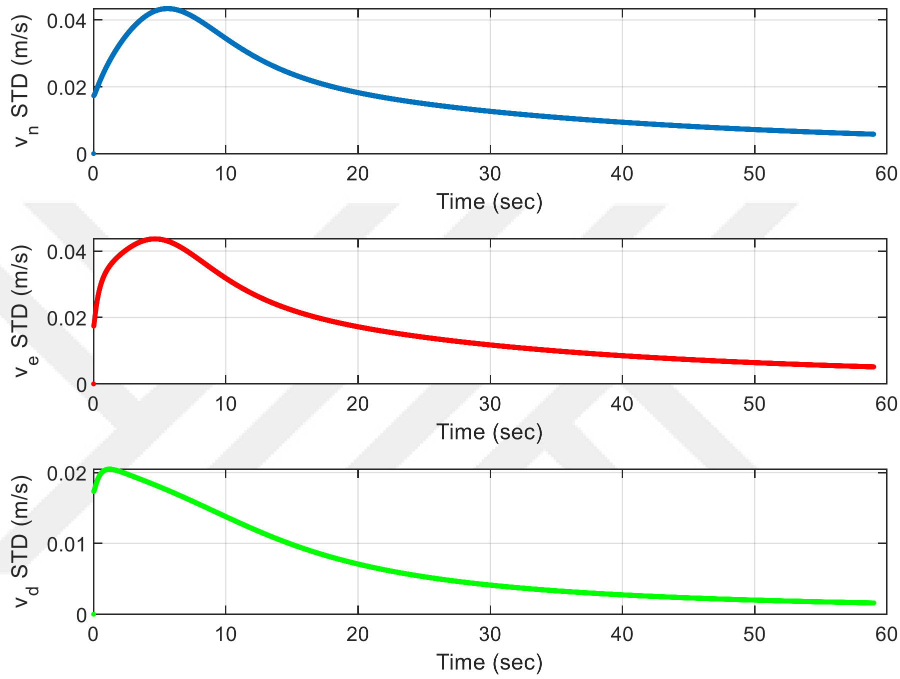

Figure 7 37**:** Velocity standard deviation (STD) behavior

Figure 7.42 shows velocity standard deviation simulation results where initially a little bit higher deviation occurs in a very short period of time in few seconds at about 5seconds and the deviation converge to approximately zero over time. This shows that the system noise and bias are very low over time and makes the system accuracy interruption to be very less.

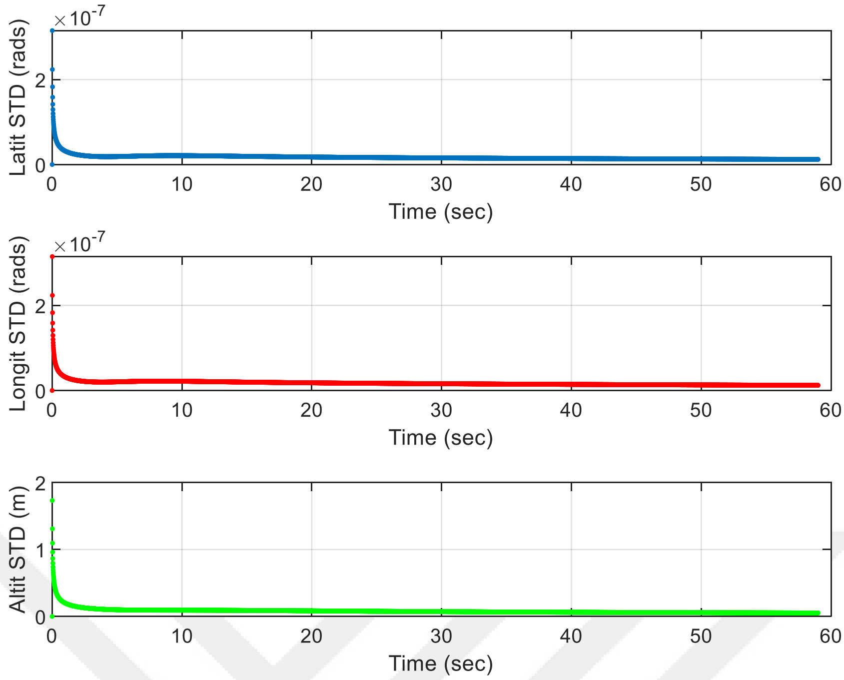

Figure 7 38**:** Aircraft position standard deviation

Based on fig 7.43, the simulated results show that all parameters give confidence in using stereo cameras/INS for relative navigation because of the in-range standard deviation propagation over time. Simulation shows that at the initial stage deviation is a litle bit high which stablely and quickly converges near to zero over time.

7.5.3 GPS/IMU Navigation Standard Deviation Behavior

Real GPS/INS is exposed to tolerable system deviation from errorless standards. The simulation shows that the less and reducing to zero orientation, position, and velocity standard deviations are shown below

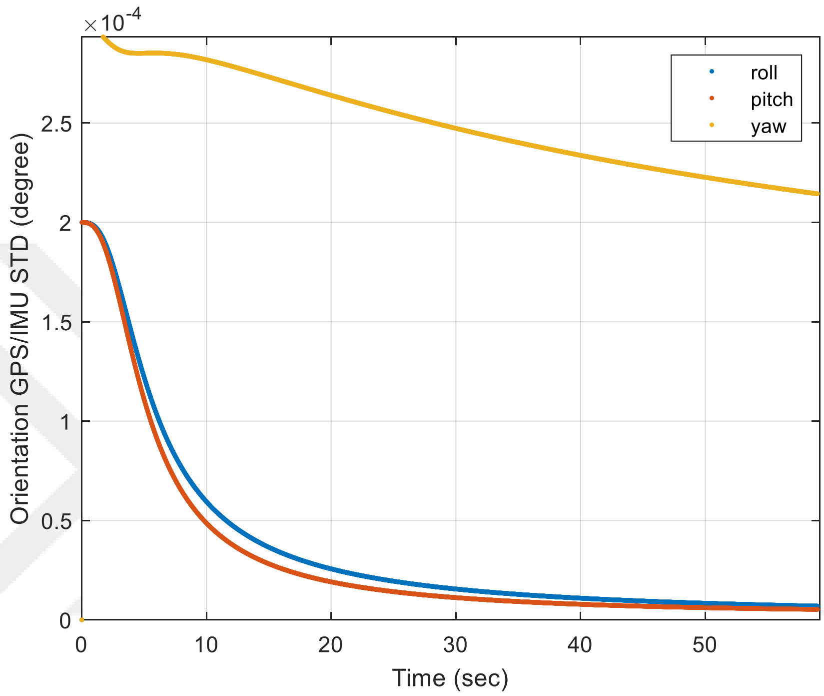

Figure 7 39**:** Orientation STD navigating with GPS/IMU

The fig 7.44 orientation simulation results show that real aircraft navigation with GPS/INS has less and in range standard deviations.

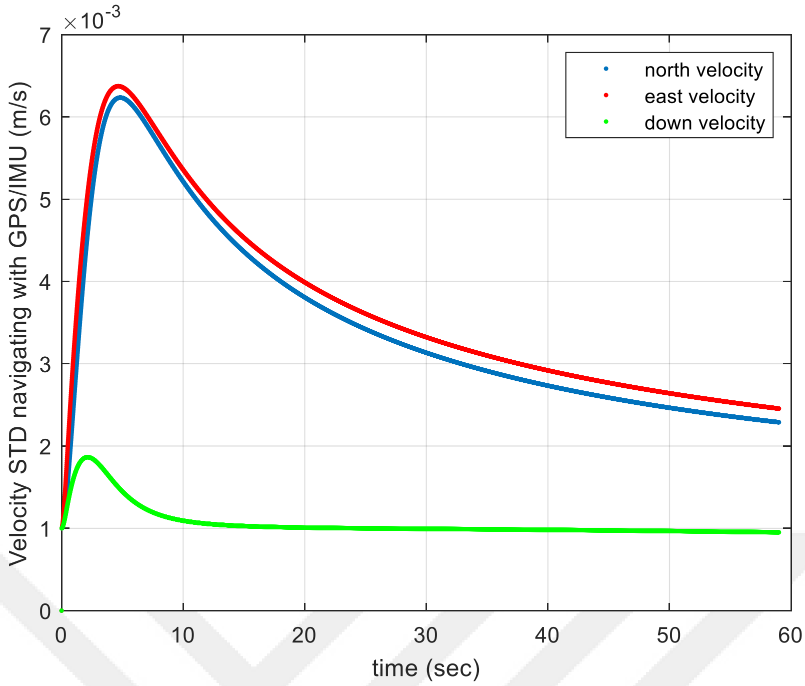

Figure 7 40**:** Velocity standard deviation

The fig 7.45 shows that the deviation in down velocity is 0.001 m/s almost throughout the time interval but at the start, the variation of deviation has increased up to 0.0018m/s in the first 5 seconds. This simulation result shows that the overall standard deviation is in its normal range. 0.006m/s north and east velocity is the shown simulation result deviation when navigating with GPS/INS.

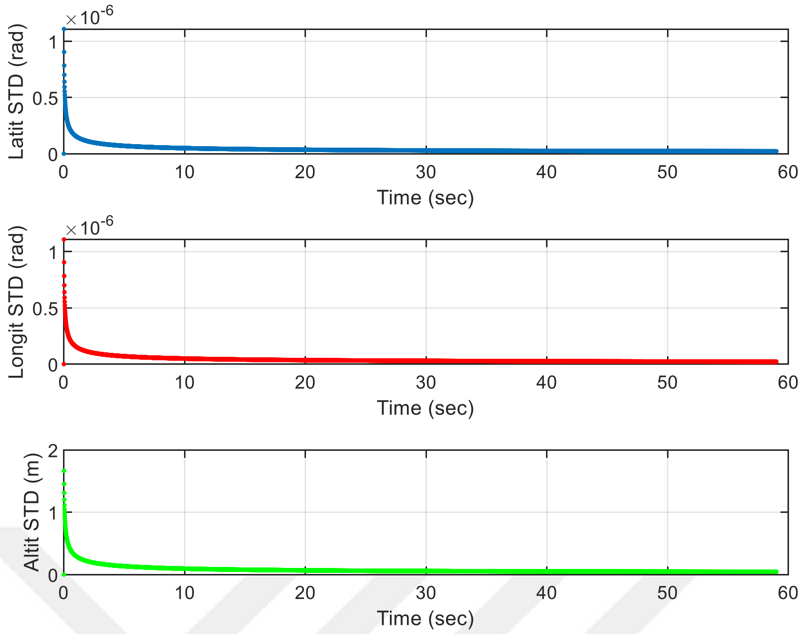

Figure 7 41**:** Position standard deviation with GPS/IMU

Fig 7.46 shows that the simulated standard deviation of an aircraft position is a bit higher at its initial stage, converges quickly to nearly zero, and stably maintains the deviation frequency.

The overall standard deviation simulated results show that the parameter variations are in the normal standard deviation range (± 2) parameter unit. This justifies that when navigating with stereo camera/IMU or navigating GPS/IMU the deviation is in the normal range therefore the deviation does not affect the navigation accuracy and safety.

CHAPTER 8

CONCLUSION AND RECOMMENDATION

8.1 Conclusion

Integration of inertial measurement units (IMU) and cameras for a vertical landing aircraft on a pattern offers a dependable and adaptable way to improve the precision and dependability of flying vehicles' relative navigation systems. Through the calculation of the difference between images taken from two separate views, stereo cameras enable real-time depth perception. Enabling the flying vehicle to safely navigate complicated terrain, this feature is essential for obstacle identification and avoidance. Stereo cameras are self signal reliance and are capable of performing navigation as much as the most useable sensors or systems like GPS. This makes stereo cameras less exposed to signal interference and less errors. Even though the calibration methods for stereo cameras which include extrinsic and intrinsic calibrations are complex, but could be achieved not like that of GPS where there is no action on satellite position and signals.

Based on the system error analysis at 200m an altitude of aircraft in 60seconds of flying simulation, the simulation shows that the stereo camera and IMU fused with extended Kalman filter provides less standard deviation and stable errors for all navigation parameters (orientation, velocity, and position) estimation of the flying vehicle over simulation time at less pitch and roll angles (not exceeding 15^0).

Apply advanced sensor fusion techniques, like the use of IMU and Kalman filtering approaches, to integrate stereo camera data with other sensors, ensuring a robust and accurate navigation solution. Integration of stereo cameras with INS can enhance navigation safety for flying vehicles at low cost where by sensor fusion approaches is able to improve the overall resilience of a system by mitigating the limitions of individual sensors.

In this study using a Matlab environment, the use of GPS, stereo camera, IMU, and extended Kalman filter were put into consideration. The form of landing considered in the study is the vertical landing of flying vehicles. At an altitude of 200 meters, the attitude of the flying vehicle was studied and compared to that treated as errorless (nominal) navigation parameters. The Matlab program and simulation comparison between INS/GPS and stereo camera/IMU was made to see the behaviors of flying vehicles in relation to nomial navigation parameters when landing on a known pattern at a given period of time. The time used when navigating with GPS/IMU and camera/IMU was all the same at the same latitude, longitude, and altitude.

The simulation analysis showed that when navigating using the stereo camera/IMU for a relative navigation system provides almost the same results as that of nominal navigation with very less system errors. The simulation results of aircraft positioning errors when using a stereo camera/IMU show 0.01m altitude, 0.0014m latitude, and 0.004m longitude which is a very very low error to the almost nominal and decrease over time while pure INS position errors keep on increasing over time.

The accuracy comparison with GPS/IMU and stereo camera/IMU navigation all showed that the use of the camera in the position of GPS could be more reliable when it does not require external signal sources in the identification of flying vehicle position, orientation, and velocity.

Improved situational awareness and navigation accuracy can be achieved by integration of stereo cameras/IMU into flying vehicles for relative navigation systems. Flying vehicles can accomplish accurate and self-dependable navigation signals, which is necessary for autonomous operation in complex and dynamic settings, by utilizing the depth perception capabilities of stereo vision and combining it with data from other sensors like IMU. Stereo cameras/IMU simulation shows diminished errors and stable errors compared to pure inertial navigation system (INS) and global positioning system (GPS)/INS real navigation. The small standard deviation over time when navigating with stereo camera/IMU fusion with an extended Kalman filter which smoothens the system bias, makes this system reliable and accurate. Stereo camera/IMU having been the self-signal dependent and stable parameter propagation over time makes it cheaper and hence reliable for relative navigation for all kinds of flying vehicles mostly at low altitudes.

8.2 Recommendation

The simulation using MATLAB was done and showed accurate results but the real field practical may show different parameter behaviors, it is in the same regard that the field practical is recommended.

There are more advanced and accurate estimation methods over the extended Kalman filter which may fuse the system and result in more accurate aircraft navigation parameters the use of more advanced nonlinear state estimation methods is recommended for further research to evaluate and analyse the aircraft behavior when landing using camera/ inertial measurement unit.

The simulation test was done in consideration of an aircraft at low altitudes and vertically landing and the results have proved the system's accuracy however the test of the system at higher altitudes and other landing stages of an aircraft is recommended for future research.

The use of scale-invariant feature transform (SIFT) and speeded-up and robust (SURF) are the most used feature detection techniques in visual odometry however there are other advanced feature detection techniques like the Harris corner detector that could be used and show more navigation accuracy, study of advanced feature detection and processing is advised for future work.

REFERENCES

[1] D. H. (David H.) Titterton, J. L. (John L.) Weston, Institution of Electrical Engineers., and American Institute of Aeronautics and Astronautics., *Strapdown inertial navigation technology*. Institution of Electrical Engineers, 2004.

[2] A. M. Fosbury and J. L. Crassidis, "Relative Navigation of Air Vehicles."

[3] R. C. Leishman, T. Mclain, R. W. Beard, R. C. ; Leishman, T. ; Mclain, and T. W. Mclain, "Relative Navigation Approach for Vision-based Aerial GPS-denied Relative Navigation Approach for Vision-based Aerial GPS-denied Navigation Navigation BYU ScholarsArchive Citation BYU ScholarsArchive Citation 'Relative Navigation Approach for Vision-based Aerial GPS-denied Navigation' (2013). Faculty Publications Relative Navigation Approach for Vision-Based Aerial GPS-Denied Navigation," 2013. [Online]. Available: https://scholarsarchive.byu.edu/facpub.1946.https://scholarsarchive.byu.edu/facpub/1946

[4] S. C. Felter, S. Member, and N. W. Eva, "A Relative Navigation System for Formation Flight."

[5] S. Nassar, X. Niu, and N. El-Sheimy, "Accurate INS/GPS Positioning with Different Inertial Systems Using Various Algorithms for Bridging GPS Outages," 2005. [Online]. Available: https://www.researchgate.net/publication/281628174

[6] S. Sukkarieh and M. George, "Tightly coupled INS/GPS with bias estimation for UAV applications." [Online]. Available: https://www.researchgate.net/publication/228996997

[7] G. T. Schmidt and R. E. Phillips, "INS/GPS Integration Architectures," 2010.

[8] A. Favenza, C. Rossi, M. Pasin, and F. Dominici, "A Cloud-based Approach to GNSS Augmentation for Navigation Services." [Online]. Available: http://www.gsa.europa.eu/#

[9] E. N. Johnson, A. J. Calise, Y. Watanabe, J. Ha, and J. C. Neidhoefer, "Real-time vision-based relative aircraft navigation," *Journal of Aerospace Computing, Information and Communication*, vol. 4, no. 4, pp. 707–738, Apr. 2007, doi: 10.2514/1.23410.

[10] R. Hartley and A. Zisserman, *Multiple view geometry in computer vision*.

[11] H. G. Asl and A. D. Firouzabadi, "Integration of the inertial navigation system with consecutive images of a camera by relative position and attitude updating," *Proc Inst Mech Eng G J Aerosp Eng*, vol. 233, no. 15, pp. 5592–5605, Dec. 2019, doi: 10.1177/0954410019852818.

[12] S. Nassar, N. El-Sheimy, and K.-P. Schwarz, "INS and INS/GPS Accuracy Improvement Using Autoregressive (AR) Modeling of INS Sensor Errors," 2004. [Online]. Available: https://www.researchgate.net/publication/281627957

[13] S. Sukkarieh and M. George, "Tightly coupled INS/GPS with bias estimation for UAV applications." [Online]. Available: https://www.researchgate.net/publication/228996997

[14] A. M. Fosbury and J. L. Crassidis, "Optimal Trajectory Determination for Increased Relative Navigation Observability of Air Vehicles."

[16] S. Silvestrini, M. Piccinin, G. Zanotti, A. Brandonisio, P. Lunghi, and M. Lavagna, "Implicit Extended Kalman Filter for Optical Terrain Relative Navigation Using Delayed Measurements," *Aerospace*, vol. 9, no. 9, Sep. 2022, doi: 10.3390/aerospace9090503.

[17] S. Konatowski, P. Kaniewski, and J. Matuszewski, "Comparison of Estimation Accuracy of EKF, UKF and PF Filters," *Annual of Navigation*, vol. 23, no. 1, pp. 69–87, Apr. 2017, doi: 10.1515/aon-2016-0005.

[18] G. T. Schmidt and R. E. Phillips, "INS/GPS Integration Architectures," 2010.

[19] Q. Zhang and R. Pless, "Extrinsic calibration of a camera and laser range finder (improves camera calibration)," in *2004 IEEE/RSJ International Conference on Intelligent Robots and Systems (IROS)*, 2004, pp. 2301–2306. doi: 10.1109/iros.2004.1389752.

[20] "Part 4 - Geometric Camera Calibration".

[21] K. Hata and S. Savarese, "CS231A Course Notes 1: Camera Models."

[22] O. Montenbruck, T. Ebinuma, E. Glenn Lightsey, and S. Leung, "A real-time kinematic GPS sensor for spacecraft relative navigation Ein GPS Sensor zur kinematischen Relativnavigation von Raumfahrzeugen in Echtzeit," 2002. [Online]. Available: www.elsevier.com/locate/aescte

[23] H. G. Asl and A. D. Firouzabadi, "Integration of the inertial navigation system with consecutive images of a camera by relative position and attitude updating," *Proc Inst Mech Eng G J Aerosp Eng*, vol. 233, no. 15, pp. 5592–5605, Dec. 2019, doi: 10.1177/0954410019852818.

[24] H. Ghanbarpourasl, “Attitude reconstruction from strap-down rate gyros using power series,” *Journal of Navigation*, vol. 74, no. 4, pp. 763–781, Jul. 2021, doi: 10.1017/S0373463321000023.

[25] S. Nassar, N. El-Sheimy, and K.-P. Schwarz, “INS and INS/GPS Accuracy Improvement Using Autoregressive (AR) Modeling of INS Sensor Errors,” 2004. [Online]. Available: https://www.researchgate.net/publication/281627957

[26] S. Nassar, X. Niu, and N. El-Sheimy, “Accurate INS/GPS Positioning with Different Inertial Systems Using Various Algorithms for Bridging GPS Outages,” 2005. [Online]. Available: https://www.researchgate.net/publication/281628174

[27] A. Noureldin, T. B. Karamat, and J. Georgy, “Basic Navigational Mathematics, Reference Frames and the Earth’s Geometry,” in *Fundamentals of Inertial Navigation, Satellite-based Positioning and their Integration*, Springer Berlin Heidelberg, 2013, pp. 21–63. doi: 10.1007/978-3-642-30466-8_2.

[28] J. M. Salacain, “Application of imaging system geometric models to a synthetic image generation system Recommended Citation.” [Online]. Available: http://scholarworks.rit.edu/theses

[30] R. Muñoz-Salinas, R. Medina-Carnicer, F. J. Madrid-Cuevas, and A. Carmona-Poyato, “People detection and tracking with multiple stereo cameras using particle filters,” *J Vis Commun Image Represent*, vol. 20, no. 5, pp. 339–350, Jul. 2009, doi: 10.1016/j.jvcir.2009.03.005.

[32] G. Sheng, X. Liu, Y. Sheng, X. Cheng, and H. Luo, “Cooperative Navigation Algorithm of Extended Kalman Filter Based on Combined Observation for AUVs,” *Remote Sens (Basel)*, vol. 15, no. 2, Jan. 2023, doi: 10.3390/rs15020533.

[33] R. Der Van Merwe, E. A. Wan, and S. I. Julier, “Sigma-point kalman filters for nonlinear estimation and sensor-fusion - Applications to integrated navigation,” in *Collection of Technical Papers - AIAA Guidance, Navigation, and Control Conference*, 2004, pp. 1735–1764. doi: 10.2514/6.2004-5120.

[34] S. Konatowski, P. Kaniewski, and J. Matuszewski, “Comparison of Estimation Accuracy of EKF, UKF and PF Filters,” *Annual of Navigation*, vol. 23, no. 1, pp. 69–87, Apr. 2017, doi: 10.1515/aon-2016-0005.

[35] H. Ghanbarpourasl and S. Zobar, “Kalman Filtering With Linear State Equality Constraints: A Method Based on Separating Variables,” *IEEE Access*, vol. 10, pp. 35460–35468, 2022, doi: 10.1109/ACCESS.2022.3163399.

[36] S.-G. Kim, J. L. Crassidis, Y. Cheng, A. M. Fosbury, and J. L. Junkins, "Kalman Filtering for Relative Spacecraft Attitude and Position Estimation."

[37] S.-G. Kim, J. L. Crassidis, Y. Cheng, A. M. Fosbury, and J. L. Junkins, "Kalman Filtering for Relative Spacecraft Attitude and Position Estimation."

[38] S. H. Pourtakdoust and H. Ghanbarpour Asl, "An adaptive unscented Kalman filter for quaternion-based orientation estimation in low-cost AHRS," *Aircraft Engineering and Aerospace Technology*, vol. 79, no. 5, pp. 485–493, 2007, doi: 10.1108/00022660710780614.